Impact of Larval Behaviors on Dispersal and Connectivity of Sea Scallop Larvae over the Northeast U.S. Shelf

Changsheng Chen[1], Liuzhi Zhao[1], Scott Gallager[2], Rubao Ji[2], Pingguo He[1], Cabell Davis[2], Robert C. Beardsley[3], Deborah Hart[4], Wendy C. Gentleman[5], Lu Wang[1], Siqi Li[1], Huichan Lin[1], Kevin Stokesbury[1], David Bethoney[6]

[1]School for Marine Science and Technology, University of Massachusetts-Dartmouth, MA 02744

[2]Department of Biology, Woods Hole Oceanographic Institute, MA 02543

[3]Depatment of Physical Oceanography, Woods Hole Oceanographic Institute, MA 02543

[4]Northeast Fisheries Science Center, NOAA, Woods Hole, MA 02543

[5]Department of Engineering Mathematics and Internetworking, Dalhousie University, Halifax, NS, Canada, B3J 1Y9

[6]Commercial Fisheries Research Foundation, RI 02874

Highlights:

- Larval swimming within the ocean mixed layer affected the interannual variability of scallop larval dispersal and settlement.
- Ignoring larval swimming behavior in the ocean mixed layer likely overestimates the larval connectivity between Georges Bank (GB) and the Middle Atlantic Bight (MAB).
- Climate-induced warming tends to alter the circulation in ways that intensify larval retention over GB and restrict larval transport from GB to the MAB.

Abstract

Sea scallops (*Placopecten magellanicus*) are a highly fecund species that supports one of the most commercially valuable fisheries in the northeast U.S. continental shelf region. Scallop landings exhibit significant interannual variability, with abundances widely varied due to a combination of anthropogenic and natural factors. By coupling a pelagic-stage Individual-Based scallop population dynamics Model (hereafter referred to as Scallop-IBM) with the Northeast Coastal Ocean Forecast System (NECOFS) and considering the persistent aggregations over Georges Bank (GB)/Great South Channel (GSC) as source beds, we have examined the dispersion and settlement of scallop larvae over 1978-2016. The results demonstrated that the significant interannual variability of larval dispersal was driven by biophysical interactions associated with scallop larval swimming behaviors in their early stages. The duration, frequency, and stimulus of larval vertical migration in the ocean mixed layer (OML) affected the residence time of larvae in the water column over GB. It thus sustained the persistent aggregations of scallops in the GB/GSC and Southern New England region. In addition to larval behavior in the OML, the larval transport to the Middle Atlantic Bight (MAB) was also closely related to the intensity and duration of northeasterly wind in autumn. There was no conspicuous connectivity of scallop larvae between GB/GSC and MAB in the past 39 years except in the autumn of 2009. In 2009, the significant larval transport to the MAB was produced by unusually strong northeasterly winds. Ignoring larval behavior in the OML could overestimate the scallop population's connectivity between GB and the MAB and thus provide an unrealistic prediction of scallop larval recruitment in the region. Both satellite-derived SST and NECOFS show that the northeast U.S. shelf experienced climate change-induced warming. The extreme warming at the shelfbreak off GB tends to intensify the cross-isobath water temperature gradient and enhance the clockwise subtidal gyre over GB. This change can increase the larval retention rate over GB/GSC, facilitating enhanced productivity on GB.

1. Introduction

Sea scallops (*Placopecten magellanicus*), which occur on the northeast continental shelf of North America, support the most valuable wild scallop fishery in the world (Shumway and Parsons, 2016). Georges Bank (GB) is one of two areas with the highest scallop abundances in the Northwest Atlantic (*Stokesbury et al*., 2004; *Hart and Rago*, 2006; *NFSC*, 2018) (Fig.1). Based on drop-camera surveys with a coverage area of 27×10^3 km^2 over the period 2016-2018, *Stokesbury and Bethoney* (2020) estimated the scallop population over the northeast shelf, accounting for ~34 billion individual scallops, ~71% of which were on GB. Over GB, the scallop landings exhibited considerable interannual variability, with an annual value of hundreds of million dollars (*Naidu and Robert*, 2006; *NFSC*, 2018). Benefiting from the implementation of closed areas as well as fishing effort and gear restrictions, U.S. sea scallop stocks rapidly recovered from a period of severe overfishing during the 1990s (*Murawski et al*., 2000; *Hart and Rago*, 2006; *Hart et al*., 2013; *Davies et a*l.. 2015; *NFSC,* 2018). However, even in light of the recovery, sea scallop abundances have varied significantly, largely due to high recruitment variability affected by a combination of anthropogenic and natural factors (*Hart and Rago* 2006; *NFSC,* 2018).

Recruitment, which is estimated by the survivorship of scallop larvae in their early life stages, is crucial in determining the population size. The early scallop life stages consist of pelagic and benthic phases. Adult scallops spawn eggs near the bottom. After external fertilization, trochophores hatch within 1-2 days, develop small cilia a few hours after hatching, and then start to migrate upward towards the sea surface (*McGarvey et al.*, 1992; *Hart and Chute*, 2004; *Cragg*, 2006). Once arriving at the sea surface, they undergo vertical migrations within the surface oceanic mixed layer (OML) (*Tremblay and Sinclair*, 1990a, 1990b; *Gallager et al*., 1996). The veliger stage is reached over 4-5 days with the development of shell velum (*Silva-Serra*, 1995; *Pearce et al*., 2004). At the ages of 30-35 days, veligers develop into pediveligers with foot and byssus development (*Stewart and Arnold*, 1994). Pediveligers can actively swim across the thermocline and descend towards the bottom for settlement (*Tremblay et al*., 1994). During this pelagic

100 phase, changes in the flow-driven larval dispersal and retention are primary factors in
101 controlling interannual variability in spatfall and abundance (*McGarvey et al*. 1993).
102 After settlement, the survivorship of spat (settled larvae) and juveniles crucially
103 influences the adult sea scallop population size and distribution (*Caddy,* 1975; *Hart and*
104 *Chute*, 2004). During this benthic phase, the substrate motility, water temperature,
105 currents/storms, predation, and starvation can affect the survivorship of newly settled spat
106 and juveniles (*Merrill and Edwards* 1976; *Larsen and Lee* 1978, *Hart* 2006, *Shank et al.*
107 2012).
108 The interannual variability of scallop abundance and recruitment on GB/GSC is
109 influenced considerably by changes in both physical and biological processes (*Hart and*
110 *Chute*, 2004). Understanding the driving mechanisms of these variabilities and their
111 connectivity with the Middle Atlantic Bight (MAB) can provide insights into the
112 biophysical reasons for persistently high scallop abundance over GB/GSC and primary
113 factors attributing to abundance reductions. It can also scientifically guide the
114 management of rotationally closed areas, optimal seeding of sea scallops, and protection
115 of seeded sea scallop's settling regions. It is a significant challenge to predict
116 environment-driven variability in the GB/GSC scallop population. The environmental
117 factors reflect the complex nonlinear physical-biological interaction processes, such as
118 global warming, climate-induced shelf-basin scale interactions, local wind/tidal mixing,
119 ocean acidification, ecosystem regime shift, and prey/predator fields, etc. (*Hart and Rago*,
120 2006; *Shank et al.* 2012; *Stokesbury et al.,* 2016; *Rheuban et al.,* 2018).
121 The sea scallop fishery in the U.S. Northeast is currently managed using fishing effort
122 limitations combined with rotational closures (*Hart and Rago* 2006). Areas are closed
123 based on observations of strong recruitment from surveys, and then reopened to fishing
124 after the scallops have grown to more optimal sizes for harvesting. There have been a few
125 modeling studies carried out to assess the marine environmental impact on recruitment
126 processes (reproduction, the timing of spawning, pre and post-settling larval stages) on
127 GB/GSC (*Tian et al*., 2009a, 2009b, 2009c; *Gilbert et al*., 2010; *Davies et al*., 2014,
128 2015) and in the MAB (*Munroe et al*., 2018*, Hart et al.*, 2020). *Tian et al.* (2009a)
129 developed a scallop population individual-based model (hereafter referred to as Scallop-
130 IBM). The model was coupled with the unstructured grid, Finite-Volume, Community

131 Ocean Model (FVCOM) for the Gulf of Maine (GoM) (hereafter referred to as GoM-
132 FVCOM) (*Tian et al*. 2009a, 2009b, 2009c). Spawning on GB in autumn, they ran this
133 coupled Scallop-IBM/GoM-FVCOM model for 1995-2005. The dispersal of simulated
134 scallop larvae varied interannually, with significant transport to the MAB (*Tian et al*.,
135 2009c). Driving a simplified passive and pycnocline-seeking, temperature-dependent,
136 scallop larval transport model by FVCOM-simulated monthly climatological flow and
137 temperature fields, *Gilbert et al*. (2010) examined the influences of flow-driven retention
138 and larval vertical migration on the larval dispersion in the GB/GSC region for both fall
139 and spring spawning seasons. They found that pycnocline-seeking behavior could alter
140 the larval dispersal by factors of 2-5, and thermal history could significantly affect the
141 planktonic larval duration.
142 The flow and temperature fields used in previous scallop larval transport simulations
143 (e.g., *Tian et al.,* 2009a, 2009b, 2009c; *Gilbert et al., 2010*) were from the first-
144 generation GoM-FVCOM for the region, which did not consider the physical processes
145 relating to regional-scale climate forcing. Specifically, the GoM-FVCOM hydrodynamics
146 missed two remote boundary conditions: 1) the advective transport from the upstream
147 Labrador Sea and the Arctic Ocean, and 2) the Gulf Stream-shelf interactions along the
148 southeastern part of the domain (Fig. 1). Regarding the population dynamics, although
149 Scallop-IBM included the pre-settling pycnocline-seeking behaviors of scallop larvae,
150 age-at-size-specific pre- and post-settling swimming within the OML or near the bottom
151 were not taken into account (*Stewart and Arnold*, 1994; *Gallager*, 1996; *Gallager et al*.,
152 1986a, 1986b,1996). Additionally, the spawning distribution for the 1995-2005
153 simulations was based only on a scallop dataset produced by video surveys from the
154 University of Massachusetts/School for Marine Science and Technology (UMASS-D/
155 SMAST) (*Stokesbury et al*., 2004). This dataset does not contain the data from either the
156 Canadian waters over the eastern flank of GB or NOAA surveys conducted
157 independently every year with records back to 1979. The larval behaviors and spatial
158 distributions of spawning are known to have a significant role in the bulk transport of
159 larvae (*Gilbert et al*. 2010). It is necessary to conduct an in-depth analysis of the
160 responses of dispersal patterns to different behaviors by using a model initialed with
161 complete coverage of spawning locations from all available scallop data.

High levels of adult biomass on GB/GCS, including the closed areas over Nantucket Lightship Closed Area (NLCA), Closed Area I (CA-I), Closed Area II (CA-II), and Habitat Area of Particular Concern (HAPC) in the northern part of CA-II are well established (*Hart and Rago* 2006; *Hart et al.* 2013; *Stokesbury et al*., 2015; *Gallager*, 2016). For data mining, we collected the scallop abundance data from NOAA, Canadian, and SMAST surveys, and expanded the database to cover a period from 1979 to 2017. For model development, we, a joint research team at UMASS-D and Woods Hole Oceanographic Institution (WHOI), developed the Northeast Coastal Ocean Forecast System (NECOFS). The 39-year (1978-2016) hindcast simulation of NECOFS was conducted using a global-regional nested FVCOM system, which improved the numerical simulation of the regional circulation by including the Gulf Stream-shelf interaction and flows from the upstream Labrador Sea and the Arctic Ocean. The availability of a complete scallop abundance dataset and 39-year NECOFS hydrodynamic fields allows us to re-examine the influences of physical processes and scallop larval behaviors on the early life stages of scallop larvae in the region. In particular, how do the Gulf Stream-shelf interaction and flows from the upstream Labrador Sea and the Arctic Ocean influence the transport of larval in GB/MAB in the context of realistic larval motility? How do these factors change the population connectivity between GB, Southern New England (SNE) shelf, and the MAB compared to previous estimates? Does the short-term vertical migration affect the dispersal and settlement of scallop larvae in their early life stages? What is the relative importance of these physical and biological factors for understanding and predicting changes due to dispersal and retention? Ultimately, could a coupled physical and individual-based fishery model reproduce and predict biophysical processes in terms of interannual variability and future management implications?

In this research, we have upgraded the Scallop-IBM with improvements of larval behavior parameterizations in the pre-settling stage and coupled it with the third version of GoM-FVCOM of NECOFS (hereafter referred to as GoM3-FVCOM). Using this upgraded coupled model, we examined the dispersal and settlement of scallop larvae with eggs spawning on GB over 39 years from 1978 to 2016. The NECOFS-produced hourly physical fields include the Gulf Stream-shelf interaction and the upstream flows from the Labrador Sea and the Arctic Ocean. The simulation aimed to assess the impacts of

various migrating larval behaviors within the surface OML on the scallop larvae's dispersal and settlement in their early life stages.

The remaining sections are organized as follows. Section 2 describes the data and the model. Section 3 presents the results of model simulations, including the discussion on the sensitivity of larval dispersal and retention to larval behaviors in constant and varying OMLs and the scallop population's connectivity between GB/GSC, SNE, and MAB. Section 4 highlights the biological and physical processes affecting the interannual variability of larval dispersal. Finally, section 5 summarizes the findings with conclusions.

2. The Coupled NECOFS-Scallop-IBM Model and Data

2.1. NECOFS

NECOFS is an integrated atmosphere, surface wave, and ocean forecast model system designed for the U.S. northeast coastal region. For the NECOFS version used in this study, the computational domain covers the continental shelf with boundaries over the northern coast of Chesapeake Bay on the south and the Scotian Shelf on the north, including a portion of the MAB (Fig. 2). NECOFS was placed in experimental 24/7 forecast operations in late 2007. The present version of NECOFS includes 1) a community mesoscale meteorological model named "Weather Research and Forecasting (WRF-AWR)"; 2) the regional ocean model of FVCOM (GoM3-FVCOM) (*Chen et al*. 2003); 3) the unstructured-grid surface wave model (FVCOM-SWAVE) with the same domain as GoM-FVCOM (*Qi et al*., 2009); 4) the Mass Coastal FVCOM with the inclusion of estuaries, inlets, harbors, and intertidal wetlands; and 5) four subdomain coupled wave-current FVCOM inundation forecast systems in Scituate, MA; Boston Harbor, MA; Hampton-Seabrook Estuary, NH, and Saco Bay, ME. The GoM3-FVCOM grid covers the scallop aggregation areas over GB/GSC, SNE, and the MAB. The grid is constructed using unstructured triangular meshes with a resolution of ~ 0.3-25 km in the horizontal and 45 layers in the vertical.

The 39-year (1978-2016) hindcast simulations of NECOFS were conducted using a global-regional nested FVCOM system with the core models of Global-FVCOM and GoM3-FVCOM (Fig. 2). Global-FVCOM is a fully coupled atmosphere-ice-wave-ocean,

unstructured-grid primitive equation global ocean model with a horizontal resolution varying from ~2 km within the Canadian Archipelago, shelfbreak, and coastal region to ~50 km in the interior open ocean. This model was driven by *a*) astronomical tidal forcing with eight constituents (M_2, S_2, N_2, K_2, K_1, P_1, O_1, and Q_1), *b*) surface wind stress, *c*) net heat flux at the surface plus shortwave irradiance in the water column, *d*) surface air pressure gradients, *e*) precipitation (P) minus evaporation (E), and *f*) river discharges (*Chen et al*., 2016; *Zhang et al*., 2016a, 2016b). A 39-year NECOFS hourly hindcast product is now available on the NECOFS Web Map Server (http://porpoise1.smast.umassd.edu:8080/ fvcomwms/). This database includes meteorological and oceanic components. The meteorological database includes hourly fields of physical variables such as wind velocity, air pressure, precipitation minus evaporation, shortwave radiation, longwave radiation, sensible and latent heat fluxes, and air temperature, etc. The oceanic database contains hourly fields of three-dimensional water currents, temperatures, salinity, horizontal/ vertical turbulent diffusion rates, and surface elevation.

The NECOFS-simulated physical fields were validated through comparisons with available observations. It has demonstrated success in capturing tidal- and shelfbreak density fronts, residual clockwise gyres, wind-driven upwelling, buoyancy-driven river plume, the Gulf Stream-shelf interaction (*e.g*., warm-core rings), and volume and mass transports entering the Gulf of Maine over the Nova Scotia shelf from the upstream Labrador Sea or even the Arctic Ocean. The model-data comparisons included 1) water elevations at tidal gauges (*Chen et al*., 2011, *Sun et al*., 2013), 2) temperature and salinity in the water column (*Li et al*., 2015), 3) hurricane and extratropical storms (*Chen et al*., 2013, *Beardsley et al*., 2013), 4) the surface currents measured by CODAR from 2000 to 2008 (*Sun et al*., 2016), and 5) upstream conditions in the Arctic Ocean (*Chen et al*., 2009; *Chen et al*., 2016; *Zhang et al*., 2016a,b). The success of scallop-IBM depends on the accuracy and reality of the flow fields predicted by the physical model. We have conducted a model-drifter comparison to validate the reliability of the FVCOM-produced flow field over 1995-2013. Six hundred eighty-four drifters were deployed in the GoM and GB regions, which returned valuable trajectory data (J. Manning, personnel communication). A non-parametric Kolmogorov-Smirnov test was used to judge “good”

and “bad” comparisons (*Van Sebille et al*., 2009). The results showed that 75% of drifters were in fair comparison with the model-predicted drifter trajectories (*Sun*, 2014). These validation experiments provide us with confidence in using the NECOFS-produced flow field to study the impact of physical processes on the interannual variability of sea scallop recruitment over GB/GSC, SNE, and MAB.

2.2. Scallop-IBM

The model used in this study is an upgraded Scallop-IBM coupled with the GoM3-FVCOM model. Scallop-IBM consists of four phases: egg, trochophore, veliger, and pediveliger (Fig. 3). Ages defined individual development in each stage: eggs <2 days, trochophores 2–4 days, veligers 5–40 days, and pediveligers > 40 days (*Stewart and Arnold*, 1994). We used fixed development times on pelagic stages under the assumption that the relatively small interannual changes in water temperature would produce insignificant modulation in larval development times. Similarly, the food limitation was not considered for larvae since that food was abundant during the pelagic stages.

Modeled larval behavior and their vertical migrations were considered for each life stage based on our empirical understanding. Eggs are spawned on the seabed, neutrally buoyant, and drift passively via vertical currents and turbulence but without vertical migration (*Culliney, 1974*; *Silva and O’Dor*, 1988; *Tremblay, 1*988; *Tremblay et al*., 1994). Trochophores have no directionality in their swimming and only randomly spin (*Tian et al*., 2009a), and so were also treated passively. Laboratory experiments have found that once the first shell formed (*prodisoconch*) and the larvae appear in a ‘D’ configuration, their gravity centers are below the velum, causing them to swim upwards across the thermocline (*Gallager,* 1993; *Gallager et al.,* 1996). Veligers are subject to horizontal drift in the surface OML above the thermocline, in which they actively switched between upward swimming and sinking to produce a distinct vertical migration pattern. Veligers are sensitive to light transitions, not to any prolonged state of light intensity like day or night (*Gallager et al*., 1996). Larvae between the ages of 5 and 40 days vertically migrate within the OML with various patterns such as thermocline-seeking aggregation (*Tremblay and Sinclair*, 1990a), diel (*Tremblay and Sinclair*, 1990b), and semidiurnal cells (*Gallager et al*., 1996; *Manuel et al*., 1996). *Tremblay and Sinclair* (1990b) used a pump to make profile samplings of scallop larval abundance at eight

stations on GB in October 1986 and 1987, respectively. Four of the stations were located in the stratified region. They observed an aggregation of bivalve scallop larvae in the thermocline at a depth of the subsurface chlorophyll maximum. In laboratory mesocosm experiments, over a diel cycle, veligers stayed near the surface at night, moved down, and remained at the thermocline during the day (Manuel et al., 1996) (Fig. 4). Over semidiurnal migration cycles, they stayed near the surface when daybreak, moved to the thermocline around noon, came up towards the surface at sunset, and were back to the thermocline around mid-night, forming bio-convective cells within the OML after dark (*Manuel et al*. 1996) (Fig.4). Larvae also respond to turbulence's ephemeral pulses greater than 10^{-7} W.Kg^{-1} by withdrawing their velum and sinking rapidly until the turbulent energy has subsided (*Pearce et al*., 1998). The currents in the GB/GSC region are dominated by the semidiurnal M_2 tidal currents. During the autumn, the thermocline varied significantly due to winds. The flow differed at the surface and thermoclines so that migration behaviors influenced larval retention. However, these extensive suites of swimming behaviors have never been captured in a model to date. In the past, the larvae were treated as particles with a random walk (*e.g*., *Stewart and Arnold*, 1994; *Tian et a*l., 2009a) or simple thermocline seeking behavior (*Gilbert et al.*, 2010; *Davies et al*., 2014, 2015; *Munroe et al.* 2018). Swimming behaviors could contribute significantly to the overall larval transport potential since they are always responding to the stimuli by changing their depth (*Gallager et al*., 1996). Late-stage pediveligers (>40 days) migrate downwards to settle on the seabed (1.7 mm s^{-1}), but may remain at the thermocline for more than 100 days and delay metamorphosis if thermal conditions are not suitable (*Pearce et al*., 1996). Such a delay in the settlement could lead to higher retention if larvae are in a gyre circulation. Mortality throughout the pelagic phase is carefully parameterized based on data and conditions provided in the literature (*e.g*., *Gallager et al*., 1986a,b, 1988; *McGarvey et al*. 1992).

The Scallop-IBM consists of a super-individual tracking equation given as

$$P_i(\vec{x}_{n+1},\ _{n+1}\ = P_i(\vec{x}_n,\ _n\ + \int_{t_n}^{t_{n+1}} \vec{v}\,(\vec{x},\quad d\ + W_b(x,y,\ _n\ \Delta\ + R_H + R_K \qquad (1)$$

where $P_i(\vec{x},$ is the egg or larval number in the *i*th super-individual at the location $\vec{x} = x\vec{\imath} + y\vec{\jmath} + z^{\rightarrow}$ at the time *t; x, y,* and *z* are the east, north and vertical axes of the

316 Cartesian coordinates; $\vec{\imath}$, $\vec{\jmath}$, and $\vec{k}$ are unit vectors in x, y and z directions; subscript n
317 represents the nth time step; $\vec{v}$ is the three-dimensional velocity vector; Δ is the time
318 step equaling $t_{n+1} - t_n$; W_b is the vertical migration speed due to larval behavior; R_H
319 and R_K are the horizontal and vertical random walks as functions of model-produced
320 horizontal and vertical diffusion coefficients. The formulations of R_H and R_K were
321 described in *Tian et al*. (2009c). Eq. (1) is solved by the 4th-order, 4-stage explicit Runge-
322 Kutta (ERK) method with the detail given in the FVCOM User Manual (*Chen et al*.,
323 2013). The time step used in larval tracking was 120 sec, with the random walk time step
324 of 6 sec.

325 The super-individual approach is commonly used in larval transport studies (*Scheffer*
326 *et al*., 1995; *Bartsch and Coombs*, 2004; *Woods*, 2005; *Tian et al.*, 2009a), which has a
327 similar meaning as the simulated larvae defined in *North et al.* (2008). A super-individual
328 was defined as an ensemble particle containing a total of 1.0×10^8 individual eggs. In the
329 Scallop-IMB, the spawning undergoes two phases before and after larval release (*Tian et*
330 *al*. 2009c), and the larval numbers in each super-individual are given as

331 $$P_i(\vec{x}, \quad = \begin{cases} N_s E_s \int_{t_o}^{t} \frac{1}{\sqrt{2\pi}\sigma} e^{-\frac{1}{2}(\frac{t-t_m}{\sigma})^2} d & \text{Spawning period} \\ P_i(n, \quad -\Delta \quad e^{-Mt} & \text{Release period} \end{cases} \quad (2)$$

332 where N_s is the total adult scallops in a spawning cell at $\vec{x}$; E_s is the total eggs spawned
333 by an individual scallop; t_o is the initial time at which the ith super-individual forms; t_m is
334 the maximum spawning time; σ is the standard deviation; Δ is the numerical integration
335 time step. M is the instantaneous mortality rate given as a constant of 0.25 d^{-1}. This
336 constant number was adopted from *McGarvey et al*. (1992) and *Tian et al*. (2009c). A
337 super-individual formed as total spawned eggs reached 1.0×10^8. The super-individual
338 approach helps us reduce the requirement for a computer's memory to handle a large
339 number of particles.

340 2.3. Data

341 We obtained the sea scallop biomass and distribution data in the study region over
342 1979-2017. The data were from three sources: 1) SMAST/UMASSD, 2) U.S. NOAA,
343 and 3) Bedford Institution of Oceanography (BIO). The SMAST/UMASSD drop camera
344 data covered 2003-2017, NOAA dredge survey data covered 1979-2017, and BIO dredge
345 survey data covered 2003-2017. The BIO data covered the survey areas on the eastern

346 flank of GB in Canadian waters. We received these data from the Bedford Institute of
347 Oceanography (BIO), Population Ecology Division (PED), Department of Fisheries and
348 Oceans (DFO), Canada.

349 2.4. Design of numerical experiments

350 We have conducted a set of the coupled scallop-IBM/NECOFS model experiments to
351 examine 1) how sensitive the dispersal and settlement of scallop larvae are to the
352 parameterizations of scallop larval behavior in the early stages, 2) how the interannual
353 variability of the subtidal circulation can influence the settlement of scallop larvae, and 3)
354 what are the physical processes affecting the larval connectivity between GB/GSC and
355 MAB. The simulation covered the period 1978-2016. Physical variables and parameters
356 include the flow-induced advection, water temperature, mixing intensity, and OML depth.
357 To distinguish the physical and biological impacts, we drove the Scallop-IBM by
358 spawning based on the multiyear-averaged abundance and distribution of adult sea
359 scallops over 1979-2017 (Fig. 5). The scallop data used to create the multiyear-averaged
360 field included video and dredge surveys from SMAST/UMASSD, NOAA, and
361 BIO/Canada. Different efficiency estimates were made for video and dredge data.

362 Adult sea scallops spawn in the spring and fall seasons, with the dominant spawning
363 in the autumn (*Posgay and Norman*, 1958). Here we only consider the fall spawning
364 season. Following the previous approach used in *Tian et al*. (2009a), in each year, we
365 specified the scallop spawning to satisfy a normal distribution starting at 00:00 GMT,
366 September 1 and ending at 24:00 GMT, October 10 (Fig. 6). Peak spawning was set on
367 September 20, with a 1-week standard deviation. The major spawning, which accounted
368 for an amount of 95% of the total spawning, was completed over four weeks, a spawning
369 time range observed in the field measurements (*Posgay and Norman*, 1958; *Posgay*,
370 1976; *Mullen and Morning*, 1986; *DiBacco et al*., 1995).

371 The simulation was repeated yearly. Each year, Scallop-IBM was integrated over
372 three months from September 1 to November 30, considering a time scale of ~40 days for
373 larval settlement. Two types of experiments were made (hereafter referred to as "Exp-I
374 and Exp-II"). For Exp-I, the model parameters were the same as those used in *Tian et al*.
375 (2009a). Active vertical migration was specified for each life stage. At the age of 2 days,
376 the larvae started migrating upward towards the surface at a speed of 0.3 mm/s. At the

age of 5 days or later, the rate of upward larval migration was decreased to 0.1 mm/s. At the age of 40 days, veligers developed into pediveligers, which actively migrated downwards to the seabed at a speed of 1.7 mm/s and settled on a suitable substrate. For Exp-II, in addition to the parameters considered in Exp-I, we included the vertical migration of scallop larvae during early stages within the surface OML following the schematic patterns shown in Fig. 4. Once larvae entered the OML, the upward larval migration speed was replaced by larval vertical migration behaviors specified in the OML in all Exp-II cases. During the spawning period in September, the water was generally well mixed in the shallow regions (< 40 m) over GB and stratified in the deeper water between tidal mixing and shelfbreak fronts (~40-100 m) on the southern flank of GB. During that period, the wind-induced surface OML could deepen to ~20-40 m in the stratified region. We included a vertical larval migration in the model to examine how this type of larval behavior may affect larval settlement after 40 days.

The numerical experiments were done for eight cases (Table 1). C#1 is defined as the case for Exp-I in which vertical migrations in the OML were not included. Exp-II was made for seven cases. C#2, C#3, C#4, and C#5 are defined as the cases with diel or semidiurnal vertical migration behavior in a fixed 10 or 30-m depth OML, respectively. C#6 and C#7 refer to the cases with diel and semidiurnal vertical migration behaviors in the physical model's predicted, spatiotemporally-varying OML. We also did an experiment by constraining larvae at the bottom of the model-predicted OML after they migrated upward to the surface at the age of 5 days, and referred it to as a " thermocline-seeking behavior" case (C#8). For C#6, C#7, and C#8, the hourly OML depth was determined by vertical profiles of the model-simulated water density through an empirical method described in Appendix A. The calculated OML depth was validated via modeled temperature, salinity, and density profiles, with examples shown in Figs. A1-A4.

3. Influences of the Surface OML on Larval Dispersal

3.1. Comparisons between the cases with and without constant thickness OMLs

The results indicate that the dispersal and settlement of scallop larvae varied significantly with scallop larval behaviors in their early stages and the thickness of the OML. It is elucidated from the abundance distributions of pediveliger settling at the seabed for the cases with and without diel or semidiurnal migration (C#1, C#2, C#3, C#4,

409 and C#5). Examples are displayed here for 2008, 2009, 2012, and 2013 simulated
410 numbers and concentrations of settled super-individual particle/larvae (Figs. 7-10).
411 During the autumn of these four years, the top of GB and in other shallow regions was
412 vertically well-mixed by tides. The OML depth in the mixed areas was equal to the local
413 water depth. In the following discussion, the positive and negative signs of the flow and
414 transport referred to *x*- and *y*-directions in rotated figures (e.g., Figs. 7-10: lower panels).
415 In 2008, for C#1, the scallop larvae were all retained on GB and the SNE shelf, with
416 about 49.1. and 50.9% settling in these two areas, respectively. The larvae were most
417 abundant on the eastern side of GSC and the northeast flank of GB as well as inside the
418 cold pool area (Fig.7f). The cold pool is a relatively uniform cold water body ($< 13^{o}$ C)
419 near the bottom that persists from spring through fall over the mid and outer shelf regions
420 (Lentz, 2017). For C#2 and C#3, for a specified 10-m OML, the diel or semidiurnal larval
421 migration in the OML strengthened the larval retention within the clockwise residual gyre,
422 resulting in 75.8 and 80.5% settling on GB/GSC, respectively (Figs. 7g, 7h). Although
423 the difference in larval retention rates on GB/GSC for these two cases was only ~4.7%,
424 the spatial distributions of settled larvae differed considerably. For C#2, highly abundant
425 larvae were settled on the western GB and within the GSC and the cold pool areas over
426 the Nantucket Shoal. For C#3, in addition to these three areas, a large portion of larvae
427 was settled down on the northern flank of GB. Without considering vertical migrations in
428 the OML, many larvae were advected southward within the cold pool to the SNE shelf,
429 with a southmost boundary off Long Island. When vertical migrations in the OML are
430 taken into account, the larvae entering the SNE significantly reduced, accounting for
431 ~24.2% for the diel migration case and 19.5% for the semidiurnal migration case. In both
432 cases, a relatively high abundance zone shifted northward and even entered the Long
433 Island Sound.
434 When the OML was deepened to 30 m, the distributions of settled larvae significantly
435 changed (Figs. 7i, 7j). The larvae tended to settle within tidal mixing and shelfbreak front
436 zones. Although the settled larval number remained high around the clockwise gyre over
437 GB, the highest larval abundance concentrated around the western and eastern shelves of
438 GSC. The settled larval number reduced to 56.2% and 71.5% on GB/GSC and increased
439 to 43.8% and 28.5% over the SNE shelf for C#4 and C#5, respectively. The OML

deepening enhanced the larval retention around the GSC, and restricted the southward larval transport from GB/GSC toward the MAB. In the diel migration case, the larvae over Nantucket Shoal were advected to the shelf break. That did not happen in the semidiurnal migration case. The differences shown in abundance for C#1-C#5 were observed alternatively from the larval density distributions shown in Figs. 7a-e).

The model predicts that the dispersal and settlement of scallop larvae varied significantly from year to year, which was evident in a comparison between 2009 and 2008. In 2009, regardless of larval vertical behaviors, many scallop larvae were advected to the SNE shelf and entered the MAB (Fig. 8). The main difference among C#1-C#5 was the distributions of larval settling locations, abundance, and pathways from GB/GSC to the MAB. The distributions of larval density in C#1, C#2, and C#3 were similar (Figs. 8f, 8g, 8h), except for the higher density spots occurring east of Long Island and over the MAB in C#2 and C#3. As the OML was deepened to 30 m, the larval dispersal dramatically changed. Over GB, a large portion of larvae was settled and concentrated within the mixed area in the diel migration case (C#4) (Fig. 8i), while they expanded to cover the most area of the bank in the semidiurnal migration case (C#5) (Fig. 8j). Furthermore, the OML deepening caused larvae to shift toward the shelfbreak on their journey to the MAB. The highest larval density was found in the MAB in C#5, but not in C#4. Although significant larvae were advected southward to the MAB, the cases with larval vertical migration behaviors in the OML still provided a higher larval retention rate on GB. In C#1, 33.0% of larvae were settled over GB/GSC. The retention rate varied with the OML depth and larval behaviors. For C#2-C$4, it was increased from 39.6% to 56.2% when the OML deepened from 10 m to 30 m, while for C#5, it remained similar for the 10- and 30-m OML cases. The features described here can be viewed alternatively from the larval density distributions for C#1-C#5 shown in Figs. 8a-e.

2012 was a warm year during which the nearshore sea temperature increased by ~1.0-2.0ºC. Warming intensified the cross-isobath gradients of the bottom temperature over the middle shelf and shelfbreak. The settlement of larvae is influenced considerably by larval behaviors in the OML and the OML depth. For C#1, many larvae were transported to the SNE shelf and even entered the MAB, with the highest abundance over GB and within the cold pool south of Long Island (Figs. 9a, 9f). When diel and semidiurnal larval

vertical migration behaviors were considered in a fixed 10-m depth OML (C#2 and C#3), the larvae over GB were aggregated around GSC, with a portion entering the SNE shelf (Figs. 9b, 9g, 9c, 9h). Although the larval distribution patterns for C#2 and C#3 were similar, the larval dispersal was more extensive in the semidiurnal migration case than in the diel migration case. As the OML depth deepened to 30 m, most larvae were retained on GB and around GSC. No larvae were advected southward to enter the MAB. For a given OML depth, the larval distributions varied with larval behaviors in the OML. For C#4, the settled larvae showed a dispersive distribution on GB, with the highest abundance in the cold pool area over Nantucket Shoal west of GSC (Figs. 9d, 9i). For C#5, the larvae were settled around the tidal-mixing front on GB, with a dense aggregation around GSC (Figs. 9e, 9j). The results for C#4 and C#5 were correlated well with the extremely high recruitment found in NLCA from 2012 (*Bethoney et al.*, 2016).

Changes in the larval dispersal and settlement with the OML depth and larval behaviors in 2013 were similar to that found in 2012 (Fig. 10). Either ignoring larval behaviors in the OML (C#1) or having larval behaviors in a thin OML (C#2 and C#3) overestimated the southward larval transport. The deeper OML favored larval retention over GB/GSC and Nantucket Shoal (C#4 and C#5). For a given 30-m OML, the larval dispersals significantly differed for the diel (C#4) and semidiurnal (C#5) migration cases. For C#4, the highest larval aggregation area was on the SNE (Figs. 10d, 10i), while for C#5, it was around the GSC (Figs. 10e, 10j). Over GB, similar to 2012, the settled larvae were distributed on the top and western areas in the C#4 case, while they occupied the entire bank in the C#5 case.

The significant difference among C#1-C#5 for 2008, 2009, 2012, and 2013 illustrates that the larval dispersal and settlement varied not only by the changes in physical environments but also with larval behaviors in the OML. Larval behaviors in the OML made larvae stay longer in the vertical column before settling, increasing the larval residence time on GB. Thus, ignoring it will overestimate the larval transport to the SNE shelf and MAB.

3.2. Influences of larval behaviors in the varying-thickness OML

The OML depth varied significantly in time and space, especially during spring and autumn (Flagg, 1987). In these two seasons, it was in a range of 10-40 m over the shelf

(*Li et al*., 2020). The vertically well-mixed and stratified areas were distinct in the model-predicted mean water density profilers throughout September-November. In 2013, for example, the water was vertically well-mixed in areas where bottom depths were shallower than 50 m over GB and Nantucket Shoal, while it was strongly-stratified on the southern flank of GB, in GSC, and over middle/outer shelves of SNE and MAB (Fig. 11). Three sections labeled A, B, and C were selected to show the variability of the OML on the eastern and southern flanks of GB and the SNE shelf over September-November (Fig. 12). Over GB, in the areas between tidal and shelfbreak fronts, the OML depth was ~10 m in September and then gradually increased to ~30-40 m or deeper in November (Fig.12: see A and B). Within the shelfbreak front, the OML depth remained steady after October. On Section-B, the OML thinned rapidly in November, suggesting a local scale onshore intrusion of the stratified Gulf Stream water during that period. The temporal variability of the OML at Section-C over the SNE shelf was similar to that at Section-A on the eastern flank of GB.

To examine the influence of larval behaviors in a varying OML on the dispersal and settlement of scallop larvae, we repeated the 2013-2016 experiments with the real-time OML provided hourly from NECOFS (C#6 and C#7). We also ran the model with a thermocline-seeking larval behavior in the same model-predicted OML (C#8). These additional cases were conducted over the same period, starting on September 1 and ending on November 30. The comparison was made among results obtained for eight cases (C#1-C#8) with and without the inclusion of larval behaviors.

The results showed that the variability of the OML had a marked influence on the scallop larval dispersal. An example was exhibited here for 2013 simulation results. Although the settled larval distributions were similar between C#6 (Figs. 13a, 13d) and C#4 (Figs. 10d, 10i) and also between C#7 (Figs. 13b, 13e) and C#5 (Figs. 10e, 10j), the spatiotemporal variation of the OML pushed larvae in the highly abundant area northward to the Nantucket Sound in C#6 (Figs. 13a, 13d) and aggregated larvae on the western shelf of GSC in C#7 (Figs. 13b, 13e). C#8 considered a case for constraining larvae at the bottom of the OML. In this case, most of the larvae aggregated on southern and western flanks of GB, within the region between 50- and 100-m isobaths (Figs. 13c, 13f). The highest larval density area was in the GSC area, but the abundance was much

533 smaller than those found for C#7. For C#7 and C#8, either semidiurnal migration or
534 thermocline-seeking behavior consistently predicted a larval aggregation in the closed
535 area around GSC. This feature was not captured in the case without larval behaviors in
536 the OML.
537 Changes in the residence time of larvae in the water column on GB were one of the
538 reasons for distinct differences in the larval dispersal and settlement for C#1-C#8. For
539 example, tracking a super-individual originating from the same initial location on GB for
540 these eight cases, we examined horizontal and vertical movements of this super-
541 individual under different biophysical environments (Fig. 14). In each case, the tracking
542 period was 41 days, with its trajectory sampled daily. For C#1, the super-individual
543 migrated upward to the sea surface at the 5-day age and then stayed there until they grew
544 to the 40-day age. The near-surface flow rapidly advected this super-individual
545 southward along the shelf, with a residence time of ~15 days on GB (Fig.14a). When
546 larval behaviors in the OML were considered, the daily larval trajectory varied with the
547 sampling method. Here sampling was taken at noon each day. At this time, the larvae
548 were mainly at the bottom of the OML regardless of diel, semidiurnal, and thermocline-
549 seeking larval behaviors.
550 For C#2 and C#3, the super-individual migrated upward to the subsurface at a depth
551 of 10 m at the 5-day age and moved southward following a daily mean trajectory at the
552 bottom of the OML (Figs. 14b, 14c). After 40 days, it settled to the seabed around GSC.
553 Compared with the diel migration behavior, the semi-diurnal migration behavior favored
554 retaining the larvae on GB, even though their trajectories almost coincided during the
555 first 7 days. As a result, the super-individual settled on the western shelf of GSC in C#2,
556 but within the GSC in C#3 (Fig. 14b).
557 Similar features were also found for C#4 and C#5 when the OML depth was
558 deepened to 30 m. In the diel vertical migration case (C#4), after the super-individual
559 migrated upward to enter the OML, it followed a daily trajectory at the bottom of the
560 OML to move southward along the bank (Fig. 14c). This super-individual then settled
561 down near the shelf break of the SNE shelf. Differing from C#4, the super-individual in
562 C#5 was trapped locally after 8 days and eventually settled around 60-m isobath area on
563 the southern flank of GB after 40 days (Fig. 14c). For a given fixed-depth OML, the

longer distance in vertical migration tended to make the larvae move slowly in the horizontal. This feature was also observed in the spatiotemporally-varying OML cases, even though horizontal and vertical trajectories of the super-individual significantly differed.

The diel vertical migration behavior (C#6) was less favorable to retain the larvae on GB compared with semidiurnal (C#7) and thermocline-seeking (C#8) vertical migration behaviors (Fig. 14d). For C#6, the super-individual followed the clockwise gyre circulation to drift along the bank during the first 35 days, then turned northward on the western GB, and eventually settled at the seabed east of the GSC. The trajectory of this super-individual varied significantly in the vertical before settling. For C#7 and C#8, the semidiurnal or thermocline-seeking vertical migration pushed the super-particle offshore toward the shelfbreak front, retained it in the deeper depth, and eventually made it settle on the southeastern flank of GB, an area close to its origin. In these two cases, the thermocline-seeking behavior was more favorable to restrain the horizontal movement than the semidiurnal behavior. It explains why similar aggregation patterns were found for C#7 and C#8 around the GSC. The comparison of horizontal and vertical trajectories of the same super-individual in these eight cases again highlights the importance of including larval behaviors in the OML in the Scallop-IBM, especially for the early life stage simulation.

3.3. Statistics and connectivity of scallop larvae over GB/GSC, SNE, and the MAB

Dividing the model domain into 2×2 km boxes, we statistically calculated the mean, percentage, and standard deviation of larval density over 39 years from 1978 to 2016 for C#1-C#5, respectively. Probability is represented by the settling percentage of larvae in each box over 39 years, ranging from 0 (0%) to 1 (100%). Standard deviation was estimated relative to the 39-year mean, which illuminated the range of the interannual variability. For C#1, the mean larval density remained high over GB/GSC and SNE, with a significant interannual variability occurring in the SNE and MAB region (Figs. 15a-c). In this case, the probability rate of larvae entering the MAB was up to 50%. For C#2 and C#3, the diel vertical larval migration tended to retain larvae over GB/GSC and SNE, with maximum interannual variability occurring over the SNE shelf and northern area of

595 the MAB (Figs. 15d-i). In these two cases, the model showed that including the larval
596 behavior in the OML considerably reduced the probability rate of larvae entering the
597 MAB. The major difference between these two cases was in the spatial distribution of
598 settled larvae over GB/GSC and SNE. In the semidiurnal case, more larvae accumulated
599 in the eastern portion of NLCA and the center of GB. For C#4 and C#5, deepening of the
600 OML favored the larval retention over GB/GSC and SNE and restricted larval transport
601 from entering the MAB, even though it happened occasionally (Figs. 15j-o). Similar to
602 the 10-m OML case, the primary difference between diel and semidiurnal migration cases
603 was in the spatial distribution of settled larvae. The semidiurnal migration behavior in the
604 OML led to denser larval accumulation in the three closed areas, especially in the
605 northern portion of CA-II over the northeastern flank of GB. Regardless of whether
606 larval swimming behaviors in the OML were considered, the SNE was a region featuring
607 the maximum larval interannual variability.
608 We estimated the percentage of larvae settling in three geographic zones of GB/GSC,
609 SNE, and the MAB (see the boundary of each zone in Fig. 1) for C#1-C#5, respectively.
610 The model consistently predicted that GB/GSC was a high retention area (Fig.16 and
611 Table 2). C#2 and C#3, also C#4 and C#5, exhibited a similar interannual variability
612 pattern. On GB/GSC, the mean differences over 1978-2016 were 7.0% between C#2 and
613 C#1, and up to 10.2 between C#3 and C#1, indicating that the semidiurnal migration
614 behavior increased the retention by ~3.2% (Fig. 16a). When the OML depth was
615 deepened to 30 m, the retention rate on GB/GSC was decreased by 3.7% for the diel
616 migration case and 7.0% for the semidiurnal migration case. The SNE shelf was also a
617 high aggregation area of scallop larvae (Fig. 16b). In this region, considering larval
618 behaviors in the OML increased the larval settlement rate. The rate became higher as the
619 OML deepened. The 39-year mean difference was 6.9% between C#2 and C#1, and 5.6%
620 between C#3 and C#1. The difference was up to 23.3% between C#4 and C#1, and
621 18.8% between C#5 and C#1.
622 The most considerable difference among C#1, C#2, C#3, C#4, and C#5 was the larval
623 settlement rate in the MAB. For C#1, the model predicted a sizeable larval transport to
624 the MAB, with a 39-year mean of 22.1% and a maximum of up to 40% (Fig. 16c). The
625 larval transport to the MAB was considerably reduced by taking larval behaviors in the

626 OML into account. Except for 2009, it was about 10% or less than for C#2 and C#3, 5%
627 or less for C#4, and close to zero for C#5. The 39-year means for C#2-C#5 were 8.2, 6.3,
628 1.8, and 0.7%, respectively. These results suggest that the GB/GSC and MAB scallop
629 populations were poorly connected by larval transport. The high scallop abundance
630 observed in the MAB might have been produced by a high recruitment rate of larvae
631 spawned in the local region.
632 We started implementing a method to determine the real-time OML depth in the
633 simulation in 2013. The experiments for varying OML were done for 2013-2016. The
634 statistics of these four-year results for C#6-C#8 showed that regardless of vertical
635 migration patterns, the GB/GSC and SNE had high scallop larval settlement, with the
636 maximum interannual variability occurring over the SNE shelf (Fig. 17, Table 3). In
637 particular, the spatiotemporal variability of the OML led to denser larval accumulation in
638 the NLCA. No larvae were advected into the MAB in all three cases of C#6, C#7, and
639 C#8. We also estimated the percentage of larvae settling in three geographic zones of
640 GB/GSC, SNE, and the MAB for these three cases and compared the results with C#5.
641 For the semidiurnal migration case, the interannual variability for C#5 and C#7 exhibited
642 a similar pattern in the GB/GSC and SNE regions (Fig. 18). The spatiotemporally-
643 varying OML produced a high retention rate on GB/GSC, with a 5.4% difference
644 between GB/CSC and SNE regions for these two cases. Also, C#7 predicted less larval
645 transport to the MAB than C#5, even the transports for both cases were close to zero. For
646 the diel migration case, although the settled larvae percentages in the GB/GSC and SNE
647 regions showed a similar variation for C#6 and C#4, the spatiotemporally-varying OML
648 produced a more favorable condition to retain the larvae on GB/GSC than the fixed-depth
649 OML. The difference was up to 9.5% between GB/GSC and SNE regions for these two
650 cases. The larval settlement showed relatively large variability in C#8. The mean
651 percentages over 2013-2016 were 62.9% over GB/GSC, 37.2% over the SNE shelf, and
652 0.0% entering the MAB.
653
654 **4. Discussion**
655 Our results indicate that the larval vertical migration in the OML can significantly
656 influence the dispersal and settlement of scallop larvae over GB/GSC and SNE, as well

as larval transport to the MAB. In the GB/GSC and SNE regions, although the 39-year mean difference was in the range of ~10% or less between C#1 and C#2-C#5, their dispersal patterns differed considerably. Vertical migration made scallop larvae stay longer in the water column on GB/GSC as compared to passive larvae, because it exposed them to different currents in the deeper water, which were slower and more cyclonic (*Werner et al.*, 1993*; Page et al*., 1999). As a result, the larvae originating from eggs spawned on GB, mainly drifted around the bank following the clockwise residual flow and eventually settled on GB and surrounding SNE areas. Only a few moved southwards to enter the MAB.

The conclusions in *Tian et al*. (2009a, 2009c) were similar to our findings for C#1 (without swimming behaviors) but very different from the results for C#2-C#8 (swimming that oscillated between subsurface depths). We believe that the difference was due to the physics and larval behaviors. *Tian et al.'s* (2009a-c) simulations did not include the Gulf Stream-shelf interaction and inflow from the upstream Labrador Sea and the Arctic Ocean. The currents used to drive the Scallop-IBM significantly differed from the NECOFS fields used in this study, especially at the shelf break where the Gulf Stream influences were significant. *Tian et al*. (2009c) implemented a thermocline-seeking larval behavior in the Scallop-IBM. They assumed that the OML depth remained constant, with thermoclines always at a depth of 23 m. Once larvae migrated to 23 m, they drifted as passive particles along with the horizontal flow at that depth. The simulation covered 1995-2005, and the results showed significant larval transport to the MAB in 1998, 2001, 2004, and 2005. Especially in 2005, the larval settlement in the MAB was even more than larvae settled over GB/GSC. Comparing our simulation results with *Tian et al*. (2009a, 2009c) for the same period 1995-2005, we found that no matter how the OML depth was specified, the models predicted a high aggregation over GB/GSC and SNE, and a weak connection between GB/GSC and the MAB. Even in 2005, the larval transport to the MAB was only around 10% for C#2 and C#3 and close or equal to zero for C#4 and C#5. Over 2013-2016, we repeated the thermocline-seeking larval behavior experiment (C#8) with a similar approach used in *Tian et al*. (2009c), but we considered the spatiotemporal variation of the OML depth (Fig.17). In this case, larval transport to the MAB was non-existent.

Tian et al. (2009c) argued that vertical migration played a less critical role in the dispersal and settlement of scallop larvae originating from GB/GSC. Their argument was based on two pieces of evidence observed by *Gallager et al*. (1996) and *Tremblay and Sinc*lair (1990a). *Gallager et al*. (1996) detected the larvae migration in the OML, aggregating twice at the sea surface during the night and at the bottom of the OML during the day (e.g., Fig. 4). The measurements were made in a thin OML of ~4 m (mesocosm). *Tian et al.* (2009c) assumed that such a short-distance vertical migration would not affect the larval dispersal since the horizontal drifting velocity zone or the residence time remained unchanged. The fact was that the OML depth varied significantly in autumn, especially during a storm event (*Li et al*., 2020). *Tremblay* and *Sinclair's* profiler sampling showed a high larval abundance within thermoclines at depths varying in the range of 12-23 m on GB. Based on this observation, *Tian et al*. (2009c) questioned whether active larval vertical migration was a general feature on GB. The fact was that profiler sampling was done at different times, and each was completed in 74 min. A few in-situ observations were not sufficient to cover the daily migration period. Small amplitude diel vertical migration was also found in a shallow area of < 25 m off Grand Mann Island in the Gulf of Maine by *Tremblay* and *Sinclair* (1990b). Therefore, it may have been premature to conclude that no vertical migration of larvae existed in the region.

The scallop larval dispersal and settlement results for cases with semidiurnal and thermocline-seeking migrations (C#7 and C#8) suggest that there was almost no larval connectivity between GB/GSC and the MAB. Although the larval distributions for these two cases differed and the settlements showed more considerable variability in C#8 than in C#7, the 4-year mean settled larval percentages in either GB/GSC or SNE regions were 5.4% or less for these two cases.

Our simulation results with larval migrations within the OML show that 2009 was a year with a significant larval transport from GB/GSC to the MAB. Since that year, the retention rate of migrating larvae in the GB/GSC and SNE regions remained a high value, with almost no larvae transporting southward into the MAB. The bottom temperature over the northeast shelf was characterized by a cold pool, forming in spring, and gradually decaying through autumn (*Lentz et al*., 2003, *Lentz*, 2017). Although this cold pool's intensity was considerably weak in autumn, it was still visible as a relatively

719 uniform cold temperature region bounded by 12-13ºC contours in Fig.19. Compared with
720 the climatological mean bottom temperature over 1978-2008 (Fig. 19a), in 2009, the cold
721 pool area expanded onshore over the SNE shelf and shrank towards the shelfbreak south
722 of Long Island (Fig. 19b). 2012 was a warm year with a ~2ºC rise of the bottom
723 temperature in the tidally well-mixed area of GB and nearshore regions (Fig. 19c).
724 Warming significantly shrank the area of the cold pool and pushed it offshore. The well-
725 defined cold pool disappeared on the southern flank of GB due to the warming-induced
726 intensification of the cross-isobath gradient of bottom temperature. This feature was
727 sustained over 2013-2016 (Fig. 19d). The cold pool functioned as an index for the
728 GB/GSC, SNE, and MAB connectivity. The weakening of the cold pool's intensity and
729 intensified cross-isobath gradient of bottom temperature tends to enhance the clockwise
730 gyre circulation over GB, which indirectly supported our finding: warming has restricted
731 the larval transport from GB/GSC to the MAB.
732 The warming tendency was evident in the satellite-derived sea surface temperature
733 (SST) change over the U.S. northeastern shelf in the past decades (Fig. 20). Significant
734 warming occurred in 2012. After that, the water remained warmer. The yearly warming
735 rate of the SST averaged over the shelf bounded at the 300-m isobath was ~0.04 over
736 1982-2020 (Fig. 20a). Assuming 2012 as a year for warming regime shift, the mean SST
737 after that was about 1.0ºC higher than the climatological SST mean averaged over 1982-
738 2011. This warming feature was captured in the NECOFS simulation. The warming rate
739 in the region varied significantly in space, with the maximum around the shelfbreak off
740 GB (Fig. 20b). We examined the NECOFS-predicted subtidal flow field in the region and
741 found a branch of the Gulf Stream that flowed northeastward towards GB. This branch
742 flow has been intensified significantly in recent years, causing extreme warming at the
743 shelfbreak off GB. As we detected in the NECOFS-simulated temperature and flow fields,
744 the warming has intensified the cross-isobath gradient of water temperature on the
745 southern flank of GB and thus strengthened the clockwise gyre over the bank.
746 The model predicted extensive southward water transports in the autumn of 2009.
747 Selecting a cross-shelf section over the SNE shelf (see the location in Fig. 1), we
748 calculated the water transport through that section over 1978-2016. Across that transect,
749 the 39-year mean transport was -0.46×10^{-3} Sv (Sv = 10^6 m^3/s). The anomaly exhibited

750 relatively large positive (northward) and negative (southward) phases in 2008 and 2009,
751 respectively, and remained positive since 2011 (Fig. 21). The anomaly's interannual
752 variability explains why the larval transport to the MAB was most extensive in 2009, and
753 no connectivity between GB/GSC and the MAB had occurred since 2010. The wind was
754 a primary driver for the sizeable southward transport in autumn of 2009. The wind
755 records at Buoy#44008 show that differing from other years, the northeasterly wind
756 prevailed over the northeast shelf during autumn of 2009, with a maximum speed of >16
757 m/s (Fig. 22). The extreme northeasterly or northerly winds tended to push the water
758 onshore. It enhanced the southward along-shelf flow under a balance between the
759 pressure gradient and earth rotation-induced Coriolis forces. The flow intensification was
760 the reason why a large number of larvae drifted to the MAB in that year. This result
761 suggests that in addition to larval vertical migration behaviors in the OML, the GB/GSC
762 and MAB connectivity also depends on the intensity and duration of northeasterly winds
763 during the fall spawning season.
764 It should be pointed out that scallop spawning over GB/GSC varies interannually.
765 This variability has not been taken into account in this study. We have not considered any
766 size-dependency of spawning either (*Davies et al*., 2014). No experiments were done for
767 the case of spawning in the MAB. as it is unlikely that the larvae could be transported
768 northward to SNE, against the prevailing southward along-shelf flow. Recent
769 observations revealed persistent warming in the region. NECOFS shows that warming
770 has produced a positive anomaly of water transport over the SNE shelf since 2011. An
771 enhanced northward flow in autumn could advect larvae in the MAB to the upstream
772 SNE region. It is worth examining these questions in the future using the 39-year hourly
773 hindcast NECOFS product, which can provide insights into the biophysical processes
774 attributing to the mixing and exchanges of larvae between the GB and MAB scallop
775 populations in the SNE region.
776 We did not consider the spring spawn in our experiments. The spawning time of sea
777 scallops varies latitudinally across its range, extending from the Strait of Belle Isle,
778 Newfoundland, to Cape Hatteras, North Carolina (*Posgay,* 1957; *Barber and Blake*, 2006;
779 Stokesbury and Bethoney, 2020). Annual autumn spawning is typical in Newfoundland
780 (*MacDonald and Thom*pson, 1986), whereas semi-annual spawning is characteristic of

781 the MAB (*DuPaul et al*., 1989). On GB, the autumn spawn is dominant, while spring
782 spawning varies in magnitude and temporally (*Chute et al*., 2012; *Hennen and Hart,* 2012;
783 *Davis et al*., 2014; *Thompson et al*., 2014; *Davis et al*., 2015). Depending on mortality
784 estimates, spring-spawning contributes minimally up to about one-third of the annual
785 total larval settlement (*Davis et al*., 2014). For example, *Chute et al*. (2012) examined 14
786 scallops with stable isotopes, 13 of which were fall spawned, including 6 from GB and
787 Nantucket Shoals. The one that was spring spawned was likely spawned in the MAB. The
788 spawning cycle, fertilization success, larval survival, and dispersion are all influenced
789 heavily by the environment. As oceanographic conditions change on GB, spring-
790 spawning may become increasingly important as it is in the MAB. It could also affect the
791 larval connectivity between the GB/GSC and the MAB like that detected by *Davies et al.*
792 (2014).
793 Our studies considered various larval swimming behaviors, which require additional
794 field confirmation. Recently, *Norton et al*. (2020) examined the impact of ocean
795 conditions on the recruitment of Dungeness crab (*Metacarcinus magister*) in the U.S.
796 Pacific Northwest. Their studies examined six swimming behaviors. Considering these
797 behaviors in a generalized linear model (GLM) with superior fits to the observations, they
798 found that the ensemble solution with various swimming behaviors in the larval IBM
799 model could improve predicting larval crab dispersion. This ensemble approach could be
800 adopted in the larval scallop simulation, especially in a condition with various
801 unconfirmed swimming behaviors.
802
803 **5. Conclusions**
804 With spawning based on multiyear-averaged abundance and distribution of adult sea
805 scallops over GB/GSC, we examined the impacts of physical processes and larval
806 swimming behaviors within the OML on the interannual variability of the scallop larval
807 dispersal and settlement in the GB/GSC, SNE, and MAB regions over 1978-2016. The
808 study was conducted using the coupled Scallop-IBM and NECOFS model. The results
809 indicate that in addition to the flow-induced advection, larval behaviors in the OML
810 significantly affected larval dispersal and settlement by altering the flow-induced
811 advection experienced at different depths. The thermocline-seeking, diel or semidiurnal

812 migration behaviors of larvae in the OML increased the larval residence time in the water
813 column over GB/GSC. These behaviors led to persistent larval aggregations in the
814 GB/GSC and SNE regions. In addition to larval behaviors, larval transports to the MAB
815 were also closely related to the intensity and duration of northeasterly wind in autumn.
816 No functional connectivity of larvae between GB/GSC and the MAB occurred in the past
817 39 years, except in the autumn of 2009, during which an extreme northeasterly wind
818 prevailed. Neglecting larval behaviors in the OML can exaggerate the connectivity scale
819 of the GB and MAB sea scallop populations. Our studies suggest this connectivity will
820 only matter in intense wind scenarios as expected with future climate change.
821 SNE is the region featuring a maximum interannual variability of larval settlement.
822 The NECOFS has captured the climate change-induced warming over the U.S.
823 northeastern shelf. The extreme warming at the shelfbreak off GB has significantly
824 intensified the cross-isobath gradient of water temperature and enhanced the clockwise
825 subtidal gyre over the bank. This change tends to increase the larval retention rate over
826 GB/GSC, suggesting higher scallop recruitment in the future.
827
828 **Appendix A: A method to calculate the thickness of the ocean mixed layer**
829 The thickness of the surface ocean mixed layer (OML) is defined as a depth above
830 which the water density remains essentially unchanged in the vertical. In practice, it is
831 usually determined using a threshold approach with a criterion relative to a reference
832 value (*e.g.*, *de Boyer Montégut et al.*, 2004). Here we introduced a method based on the
833 density profile.

834 Defining H as the bathymetric depth at a particular geographic location, ρ as the
835 water density that varies vertically from $\boldsymbol{z = 0}$ at the surface to $\boldsymbol{z = -H}$ at the bottom
836 and ρ_o as the surface water density, we can estimate the mixed layer depth ($\boldsymbol{h_m}$ by

837 $$\boldsymbol{h_m = H - \sqrt{2h_{diff}/\gamma}} \quad \text{(A.1)}$$

838 where $\boldsymbol{h_{diff} = h - \rho_o H}$; $\boldsymbol{h = \int_{-H}^{0} \rho dz}$; and γ is defined as the maximum increase rate of
839 the density with depth. Once γ is determined from a density profile, we can precisely
840 estimate h_m. To demonstrate how this method work, examples are given below for three
841 idealized cases.

842 Case 1: A vertically well-mixed case with a density profiler shown in Fig. A1. In this
843 case, ρ is constant throughout the water column, so that

844 $$\boldsymbol{\rho = \rho_o;\ h = \rho_o H;\ \text{and}\ h_{diff} = 0}.$$

845 Substituting h and h_{diff} into (A.1), we have $h_m = H$. Note here that γ = 0. For a real
846 application, one can directly assume h_m equals the local depth.

847 Case 2: A stratified case with a linear density profiler shown in Fig. A2. In this case,

$$\boldsymbol{\rho = \rho_o - (\rho_H - \rho_o\ z/H}.$$

Substituting it into (A.1), we have

848 $$\boldsymbol{h = \int_{-H}^{0}[\rho_o - (\rho_H - \rho_o\ z/H]dz = (\rho_H + \rho_o\ z/H;\ h_{diff} = 0.5\ (\rho_H - \rho_o\ H}.$$

849 Also, $\boldsymbol{\gamma = (\rho_H - \rho_o\ /H}$, so that $\boldsymbol{h_m = H - \sqrt{2h_{diff}/\gamma} = 0}$.

850 Case 3: A two-layer with a density profiler shown in Fig. A3. In this case, the density
851 profiler is given as

852 $$\boldsymbol{\rho = \begin{cases} \rho_o, & -h_m \le z \le 0 \\ \rho_o - (\rho_H - \rho_o\ (z + h_m\ /(H - h_m\ , & z \le -h_m \end{cases}}$$

853 and $\boldsymbol{\gamma = (\rho_H - \rho_o\ /(H - h_m\ }$, then, we have

854

$$\boldsymbol{h = \rho_o h_m + 0.5\,(\rho_H + \rho_o\ \ (H - h_m}$$

and

$$\boldsymbol{h_{diff} = h - \rho_o H = \frac{\rho_H - \rho_o}{2}(H - h_m\ ,}$$

so that

$$\boldsymbol{h_m = H - \sqrt{2h_{diff}/\gamma} = H - (H - h_m\ \ = h_m.}$$

With demonstrations from these three idealized cases, we applied this method to calculate the thickness of the OML based on the NECOFS-produced hourly density profile. The result was validated by comparing it with the simulated temperature, salinity, and density profiles at nodes of the triangular mesh. Examples are shown in Fig. A4 for selected three sites across GB. Using (A.1), we calculated h_m at these sites. They equaled 14.8, 5.0, and 9.1 m, respectively. Marking the calculated h_m using red dashed lines in the profiles, we found that they matched well with the depth of model-simulated OML.

Acknowledgment

This work was supported by the NOAA RSA Program with grant number NA17NMF-4540042 for C. Chen, L. Zhao, P. He, R. C. Beardsley, and S. Gallager, NA19NMF450023 for C. Chen, P. He, R. C. Beardsley, and K. Stokesbury, NOAA Fishery Climate Program with grant number NA17OAR4310273 for R. Ji and C. Davis, with WHOI subcontract number A101376 for C. Chen, and L. Zhao. The NOAA-funded IOOS NERACOOS program supported the NECOFS product under subcontract numbers NA16NOS0120023**,** NERACOOS A007, and NERACOOS A008. W. C. Gentlemen was supported by the Natural Science and Engineering Research Council of Canada. We thank the Department of Fisheries and Oceans (DFO), Canada, for providing Canadian scallop survey data. We also would like to thank Jessica Sameoto and Freya Keyser in DFO for their kindly helps in creating and delivering a well-organized Canadian dataset available to us and NOAA scientists and staff who made the NOAA dredge survey data available for this study. Dr. Brian Rothschild has given many valuable suggestions and comments on our works. His help is greatly appreciated. We also want to thank two

884 reviewers for their constructive comments and suggestions, which helped improve the
885 quality of this paper.

886 **References**

887 Barber B. J. Blake, N. J., 2006. Reproductive physiology. In: *Shumway SE (ed) Scallops*:
888 *biology, ecology and aquaculture*. Elsevier, Amsterdam, p 377-428.

889 Bartsch, J., Coombs, S. H., 2004. An individual-based model of the early life history of
890 mackerel (*Scomber scombrus*) in the eastern North Atlantic, simulating transport,
891 growth, and mortality. *Fisheries Oceanography* 13, 365–379.

892 Beardsley, R. C., Chen, C., Xu, Q., 2013. Coastal flooding in Scituate (MA): a FVCOM
893 study of the Dec. 27, nor'easter. *J. Geophys. Res.-Oceans,* 118, doi: 10.1002/
894 2013JC008862.

895 Bethoney N. D., Asci, S. C., Stokesbury, K. D. E., 2016. Implications of extremely high
896 recruitment events into the US sea scallop fishery. *Mar. Ecol. Prog. S*er. 547,
897 137-147.

898 Caddy, J. F., 1975. Spatial model for an exploited shellfish population, and its application
899 to the Georges Bank scallop fishery. *Journal of Fisheries Research Board of*
900 *Canada* 32, 1305-1328.

901 Chen, C., Liu, H., Beardsley, R. C., 2003. An unstructured, finite-volume, three-
902 dimensional, primitive equation ocean model: application to coastal ocean and
903 estuaries. *Journal of Atmospheric and Oceanic Technology* 20, 159-186.

904 Chen, C., Huang, H., Beardsley, R. C., Xu, Q., Limeburner, W. Cowles, G. W., Sun, Y.,
905 Qi, J., Lin, H., 2011. Tidal dynamics in the Gulf of Maine and New England Shelf:
906 An application of FVCOM. *J. Geophys. Res.*-Oceans 116, C12010, doi:
907 10.1029/2011 JC007054.

908 Chen, C., Beardsley, R. C., Cowles, G., Qi, J., Lai, Z., Gao, G., Stuebe, D., Liu, H., Xu,
909 Q., Xue, P., Ge, J., Ji, R., Hu, S., Tian, R., Huang, H., Wu, L., Lin, H., Sun, Y.,
910 Zhao, L., 2013. An unstructured-grid, finite-volume community ocean model
911 FVCOM user manual (4th edition), *SMAST/UMASSD Technical Report-13-0701*,
912 University of Massachusetts-Dartmouth, pp 404.

913 Chen, C., Gao, G., Zhang, Y., Beardsley, R. C., Lai, Z., Qi, J., Lin, H., 2016. Circulation
914 in the Arctic Ocean: Results from a high-resolution coupled ice-sea nested

915 Global-FVCOM and Arctic-FVCOM system. *Progress in Oceanography* 141
916 (2016), 60-80, doi: 10.1016/j.pocean.2015.12.002.
917 Chen, C., Gao, G., Qi, J., Proshutinsky, A., Beardsley, R. C., Kowalik, Z., Lin, H.,
918 Cowles, G., 2009. A new high-resolution unstructured grid finite volume Arctic
919 Ocean model (AO-FVCOM): An application for tidal studies. Journal of
920 Geophysical Research-Oceans 114, C08017, https://doi.org/10.1029/2008JC00
921 4941.
922 Culliney, J. L., 1974. Larval development of the giant sea scallop *Placopecten*
923 *magellanicus* (Gmelin). *Biological Bulletin*, 147,321-33
924 Chute A. S., Wainwright, S. C., Hart, D. R., 2012. Timing of shell ring formation and
925 patterns of shell growth in the sea scallop *Placopecten magellanicus* based on
926 stable oxygen isotopes. *Journal of Shellfish Research*, 31(3), 649-662.
927 Cragg, S. M., 2006. Development, physiology and ecology of scallop larvae. In: S.E.
928 Shumway and G.J. Parsons (Eds.) Scallops: *Biology, Ecology and Aquaculture.*
929 *Elsevier, Amsterdam*, pp. 45-122.
930 Davis, K. T. A., Gentlemen, W. C., Johnson, C. L., DiBacco, C. 2014. Relative
931 contribution of bi-seasonally spawned larvae to scallop population connectivity
932 on Georges Bank: importance of the spring spawns. *Mar. Ecol. Prog. Ser.*, doi:
933 10.3354/meps 10975
934 Davies, K. T. A., Gentlemen, W. C., DiBacco, C., Johnson, C. L., 2015. Fisheries closed
935 area strengthen scallop larval settlement and connectivity among closed areas and
936 across international open fishing grounds: a model study. Environmental
937 Management, pp.16, doi: 10.1007/s00267-015-0526-9.
938 de Boyer Montégut, C., Madec, G., Fischer, A. S., Lazar, A., Iudicone, D., 2004. Mixed
939 layer depth over the global ocean: an examination of profile data and a profile-
940 based climatology, *J. Geophys. Res.-Oceans* 109, C12003. doi:10.1029/2004JC00
941 2378.
942 DiBacco, C., Robert, G., Grant, J., 1995. Reproductive cycle of the sea scallop,
943 Placopecten magellanicus (Gmelin, 1791), on northeast-ern Georges Bank.
944 *Journal of Shellfis*h *Research* 14: 59–69.

945 DuPaul W., Kirkley, J., Schmitzer, .A, 1989. Evidence of a semiannual reproductive
946 cycle for the sea scallop, *Placopecten magellanicus* (Gmelin, 1791), in the mid-
947 Atlantic region. *Journal of Shellfish Research*, 8, 173-178.
948 Flagg, C. N., 1987. Hydrographic structure and variability. In: *Georges Bank*, R. H.
949 Backus, ed, the MIT Press, 108-124.
950 Gallager, S. M., Mann, R., 1986a. Growth and survival of larvae of *Mercenaria*
951 *mercenaria* (L.) *Crassostrea virginica* (Gmelin) and *Placopecten magellanicus*
952 relative to lipid content of eggs and broodstock conditioning. *Aquaculture* 56(2):
953 105-121.
954 Gallager, S. M., Mann, R., Sasaki, G. L., 1986b. Lipid as an index of growth and viability
955 in three species of bivalve larvae. *Aquaculture* 56(2), 81-103.
956 Gallager, S. M., 1988. Visual observations of particle manipulation during feeding in
957 larvae of bivalve molluscs. *Bull. Mar. Sci.* 43(3), 344-365.
958 Gallager, S. M., 1993. Hydrodynamic disturbances produced by small zooplankton: a
959 case study for veliger larvae of bivalve molluscs. *J. Plankton Res*. 15(11), 1277-
960 1296.
961 Gallager, S. M., 1996. Ciliary suspension-feeding and particle selection in mollusc larvae.
962 *J. Shellfish Res.*15(2), 506-510.
963 Gallager, S. M., Manuel, J. L., Manning, D. A., O'Dor, R., 1996. Ontogenetic changes in
964 the vertical distribution of scallop larvae *Placopecten megellanicus* in 9 m-deep
965 mesocosms as a function of light, food, and temperature stratification. *Mar.*
966 *Biol.*124, 679-692.
967 Gallager, S. M, 2016. Report to the Scallop PDT August 30, 2016 on scallop resource
968 and biomass in the Closed Area II HAPC. NEFC website http://www.nefmc.org/.
969 Gilbert, C. S., Gentleman, W. C., Johnson, C. L., DiBacco, C., Pringle, J. M., Chen, C.,
970 2010. Modelling dispersal of sea scallop (*Placopecten magellanicus*) larvae on
971 Georges Bank: The influence of depth-distribution, planktonic duration and
972 spawning seasonality. *Progress in Oceanography* 87(1-4), pp.37-48.
973 Hart, D. R., 2006. Effects of sea stars and crabs on sea scallop *Placopecten magellanicus*
974 recruitment in the Mid-Atlantic Bight (USA). *Marine Ecology Progress Series*
975 306, pp.209-221.

976 Hart, D. R., Rago, P. J., 2006. Long-term dynamics of U.S. Atlantic sea scallop
977 *Placopecten magellanicus* populations. *N. Am. J. Fish. Manag*. 26, 490-501,
978 https://doi.org/10.1577/ M04-116.1.
979 Hart, D. R., Chute, A. S., 2004. Essential Fish Habitat Source Document: Sea Scallop,
980 *Placopecten magellanicus*, Life History and Habitat Characteristics, 2nd Ed.
981 NOAA Tech. Mem. NMFS-NE-189.
982 Hart, D. R., Jacobson, L. D., Tang, J., 2013. To split or not to split: assessment of
983 Georges Bank sea scallops in the presence of marine protected areas. *Fisheries*
984 *Research*, 144, 74-83.
985 Hart, D. R., Munroe, D. M., Caracappa, J. C., Haidvogel, D., Shank, B. V., Rudders, D.
986 B., Klinck, J. M., Hofmann, E. E., Powell, E. N., 2020. Spillover of sea scallops
987 from rotational closures in the Mid-Atlantic Bight (United States). *ICES J. Mar.*
988 *Sc.i*, 77(5), 1992-2002.
989 Hennen, D. R., Hart, D. R., 2012. Shell height-to-weight relationships for Atlantic sea
990 scallops (*Placopecten magellanicus*) in offshore U.S. waters. *Journal of Shell*fish
991 *Research*, 31(4), 1133-1144.
992 Larsen, P. F., Lee, R. M., 1978. Observations on the abundance, distribution and growth
993 of postlarval sea scallop, *Placopeten magellanicus*, on Georges Bank. *The*
994 *Nautilus* 92, 112-116.
995 Leising, A. W., J. J. Pierson, S. Cary, B. W. Forst, 2005. Copepod foraging and predation
996 risk within the surface layer during night-time feeding forays. Journal of Plankton
997 Research 27(10), 987-1001, doi: 10.1093/plankt/fbi084.
998 Lentz, S. J. 2017. Seasonal warming of the Middle Atlantic Bight Cold Pool. *Journal of*
999 *Geophysical Research: Oceans*, 122(2):941–954, https://doi.org/10.1002/2016
1000 JC012201.
1001 Lentz, S., Shearman, K., Anderson, S., Plueddemann, A., Edson, J., 2003. Evolution of
1002 stratification over the New England shelf during the Coastal Mixing and Optics
1003 study, August 1996–June 1997, *J. Geophys. Res.-Oceans* 108(C1), 3008, doi:10.
1004 1029/2001JC001121.

Li, Y, Fratantoni, P. S., Chen, C., Hare, J., Sun, Y., Beardsley, R. C., Ji, R., 2015. Spatia-temporal patterns of stratification on the Northwest Atlantic shelf. *Prog. Oceanogr*. 134, 123-127.

Li, S., Chen, C., Wu, Z., Beardsley, R. C., and Li, M., 2020. Impacts of oceanic mixed layer on hurricanes: A simulation experiment with Hurricane Sandy. *J.. Res.-Oceans*, 125, e2019JC015851. https://doi.org/10.1029 /2019JC015851

MacDonald, B. A., Thompson, R. J., 1986. Influence of temperature and food availability on the ecological energetics of the giant scallop *Placopecten magellanicus*. III. physiological ecology, the gametogenic cycle and scope for growth. *Mar Biol.,* 93, 37-48.

Manuel, J. L., Gallager, S. M., Pearce, C. M., Manning, D. A. O'Dor, R. K., 1996. Veligers from different populations of sea scallop Placopecten magellanicus have different migration patterns. Mar. Ecol. Prog. Ser., 142, 147-163.

McGarvey, R., Serchuk, F. M., McLaren, I. A., 1992. Statistics of reproduction and early life history survival of the Georges Bank sea scallop (*Placopecten magellanicus*) population. *J. Northwest Atl. Fish. Sci.* 13, 83-99.

McGarvey, R., Serchuk, F. M., McLaren, I. A., 1993. Spatial and parent-age analysis of stock-recruitment in the Georges Bank sea scallop (*Placopecten magellanicus*) population. *Can. J. Fish. Aquat. Sci.* 50, 564-574.

Merrill, A. R., Edwards, R. L., 1976. Observation on mollusks from a navigation buoy with special emphasis on the sea scallop *Placopecten magellanicus*. *The Nautilus* 90, 54-61.

Mullen D. M., Morning, J. R., 1986. Species profiles: Life histories and environmental requirements of coastal fishes and invertebrates (North Atlantic) sea scallop. *Biological Report of US Fish Wildlife Service*, 1986, 21p.

Munroe, D. M., Haidvogel, D., Caracappa, J. C., Klinck, J. M., Powell, E. N., Hofmann, E. E., Shank, B. V., Hart, D. R., 2018. Modeling larval dispersal and connectivity for Atlantic sea scallop (*Placopecten magellanicus*) in the Middle Atlantic Bight. *Fisheries Research* 208, pp.7-15.

1034 Murawski, S. A., Brown, R., Lai, H. L., Rago, P. J., Hendrickson, L., 2000. Large-scale
1035 closed areas as a fishery-management tool in temperate marine systems: The
1036 Georges Bank experience. *Bulletin of Marine Science* 66, 775-798.
1037 Naidu, K. S., Robert, G., 2006. Fisheries sea scallop. *Placopecten magellanicus*. In:
1038 *Shumway S. E., Parsons G.J. (eds) Scallops: biology, ecology and aquaculture*.
1039 Elsevier, Amsterdam, p 869–905.
1040 North, E. W., Schlag, Z., Hood, R. R., Li, M., Zhong, L., Goss, T., Kennedy, V. S., 2018.
1041 Vertical swimming behavior influences the dispersal of simulated oyster larvae in
1042 a coupled particle-tracking and hydrodynamic model of Chesapeake Bay. Mar.
1043 Ecol. Pro. Ser., 359. 99-115. doi: 10.3354/meps07317.
1044 Northeast Fisheries Science Center (NFSC), 2018. 65th Northeast Regional Stock
1045 Assessment Workshop (65th SAW) Assessment Report. US Dept Commer,
1046 Northeast Fish. Sci. Cent. Ref. Doc. 18-08, 43 pp.
1047 Norton, E., Siedlecki, S. A., Kaplan, I. C., Hermann, A. J., Fisher, J., Morgan, C., Officer,
1048 S., Saenger, C., Alin, S. A., Newton, J., Bednarsek, N., and Feely, R.A., 2020.
1049 The importance of environmental exposure history in forecasting Dungeness crab
1050 megalopae, occurrence using J-SCOPE, a high-resolution model for the US
1051 Pacific Northwest. *Frontiers in Marine Science*, 7, 102.
1052 Page, F. H., Sinclair, M., Naimie C. E., Loder, J. W., Lozier, R. J., Berrien, P. L., Loug,
1053 R. G, 1999. Cod and haddock spawning on Georges Bank in relation to water
1054 residence times. Fish Oceanogr. 8: 212-226.
1055 Pearce, C. M., O'Dor, R.. K., Gallager, S. E., Manning, D. A., Bourget, E., 1996.
1056 Settlement of sea scallop *Placopecten magellanicus* larvae in 9 m deep
1057 mesocosms as a function of food distribution, thermoclines, depth, and substratum.
1058 *Mar. Biol.* 124(4), 693-706.
1059 Pearce, C. M., Gallager, S. M., Manning, D. A., O'Dor, R. K., Bourget, E., 1998. Effect
1060 of thermoclines and turbulence on depth of larval settlement and spat recruitment
1061 of the giant scallop *Placopecten magellanicus* larvae in 9 m-deep laboratory
1062 mesocosms. *Mar. Ecol. Progr. Ser.* 165, 195-215.
1063 Pearce, C. M., J. L. Manuel, J. L., S. M. Gallager, S. M., D. A. Manning, D. A., R. K.
1064 O'Dor, R. K., Bourget, E., 2004. Depth and timing of settlement of veligers from

different populations of giant scallop, *Placopecten magellanicus* (Gmelin), in thermally stratified mesocosms. *Journal of Experimental Marine Biology and Ecology* 312, 187-214.

Posgay, J. A., 1957. The range of the sea scallop. *The Nautilus*, 71, 55-57.

Posgay, J. A., 1976. Population assessment of the Georges Bank sea scallop stocks. *ICES Document CM* 1976/K: 34.

Posgay, J. A., Norman, K. D., 1958. An observation on the spawning of the sea scallop, *Placopecten magellanicus* (Gmelin), on Georges Bank. *Limnology and Oceanography* 3: 478.

Qi, J., Chen, C., Beardsley, R. C., Perrie, W., Cowles, G. W., Lai, Z., 2009. An unstructured-grid finite-volume surface wave model (FVCOM-SWAVE): implementation, validations and applications. *Ocean Modelling*, doi:10.1016/ j.ocemod.2009.01.007.

Rheuban, J. E., Doney, S. C., Cooley, S. R., Hart, D. R., 2018. Projected impacts of future climate change, ocean acidification, and management on the US Atlantic sea scallop (*Placopecten magellanicus*) fishery. *PLoS One* 13(9), p.e0203536.

Scheffer, M., J. M. Baveco, J. M., D. L. DeAngelis, D. L., K. A. Rose, K. A., and E. H. Van Nes, E. H., 1995. Super-individual a simple solution for modeling large populations on an individual basis. *Ecological Modelling* 80: 161–170.

Shank, B. V., Hart, D. R., Friedland, K., D., 2012. Post-settlement predation by sea stars and crabs on the sea scallop in the Mid-Atlantic Bight. *Marine Ecology Progress Series* 468, pp.161-177.

Shumway, S. E., Parsons, G. L. (eds.). 2016. *Scallops, Biology, Ecology, Aquaculture, and Fisheries*. Elsevier, Amsterdam, Oxford and Cambridge. 1214 pp.

Silva-Serra, M. A., 1995. Early life history traits of *Placopecten magellanicus* (Gmelin): behaviours, lipid condition and vertical distribution of veligers at micro- and meso-scales. Ph.D. thesis, Dalhousie University, Halifax, Nova Scotia, Canada.

Silva M. A. and R. K. O'Dor, 1988. Active depth regulation by the sea scallop larvae of *Placopecten magellanicus*? Bulletin of the Canadian Society of Zoologists, 19(2), 36p (Abstract).

1095 Sinclair, M., 1988. Marine Populations: An essay on population regulation and speciation.
1096 Washington Sea Grant Program, 252 pp.
1097 Stewart, P. L. Arnold, S. H., 1994. Environmental requirements of the sea scallop
1098 (*Placopecten magellanicus*) in eastern Canada and its response to human impacts.
1099 *Can. Tech Rep. Fish. Aquat. Sci.* 2005, 1– 36.
1100 Stokesbury, K. D. E., Harris, B. P., Marino II, M. C., Nogueira, J. I., 2004. Estimation of
1101 sea scallop abundance using a video survey in off-shore USA waters. *J. Shellfish*
1102 *Res*. 23, 33-44.
1103 Stokesbury, K. D. E., Chen, C., He, P., Zhao, L., Harris, B. P., 2015. Survey of persistent
1104 scallop aggregation and an examination of their influence on recruitment using
1105 the FVCOM oceanographic model. Final report of Sea Scallop Research under
1106 NOAA Grant Number: NA13NMF4540017.
1107 Stokesbury, K. D. E., O'Keefe, C. E., Harris, B. P., 2016. Fisheries Sea Scallop,
1108 *Placopecten magellanicus*. In S. E. Shumway and G.J. Parsons, editors. Scallops:
1109 biology, ecology and aquaculture. Amsterdam: Elsevier. Pp719-732.
1110 Stokesbury K. D. E, Bethoney, N. D., 2020. How many sea scallops are there and why
1111 does it matter? *Frontier in Ecology and Environment*, doi: 10.1002/fee.2244.
1112 Sun, Y., 2014. Long-and short-term oceanographic responses to atmospheric forcing over
1113 the Gulf of Maine and New England Shelf. Ph.D. Thesis, University of
1114 Massachusetts, 209 pp.
1115 Sun, Y., Chen, C., Beardsley, R. C., Xu, Q., Qi, J.: Lin, H., 2013. Impact of current-wave
1116 interaction on storm surge simulation: A case study for Hurricane Bob. *J.*
1117 *Geophys. Res.-Oceans* 118, 2685-2701, doi:10.1002/jgrc.20207.
1118 Sun, Y., Chen, C., Beardsley, R. C., Ullman, D., Butman, B., , Lin, L., 2016. Surface
1119 circulation in Block Island Sound and adjacent coastal and shelf regions: A
1120 FVCOM-CODAR comparison. *Progress in Oceanography* 143 (2016), 26–45.
1121 Thompson, K. J., Inglis, S. D., Stokesbury, K. D. E., 2014. Identifying spawning events
1122 of the sea scallop Placopecten magellanicus on Georges Bank. *Journal of*
1123 *Shellfish Research*, 33(1), 77-87.
1124 Tian, R. C., Chen, C., Stokesbury, K. D. E., Rothschild, B. J., Xu, Q., Hu, S., Cowles, G.
1125 W., Harris, B. P., Marino II, M. C., 2009a. Dispersal and settlement of sea scallop

1126 larvae spawned in the fishery closed areas on Georges Bank. *ICES Journal of*
1127 *Marine Sci*ence 66(10), 2155-2164, doi: 10.1093/icesjms/fsp175.
1128 Tian, R. C., Chen, C., Stokesbury, K. D. E., Rothschild, B. J., Xu, Q., Cowles, G. W.,
1129 Harris, B. P., Marino II, M. C., 2009b. Sensitivity analysis of sea scallop
1130 (*Placopectenm agellanicus*) larvae trajectories to hydrodynamic model
1131 configuration on Georges Bank and adjacent coastal regions. *Fish. Oceanogr*. 18,
1132 173-184.
1133 Tian, R. C., Chen, C., Stokesbury, K. D. E., Rothschild, B. J., Cowles, G. W., Xu, Q.,
1134 Harris, B. P., Marino II., M. C., 2009c. Modeling the connectivity between sea
1135 scallop populations in the Middle Atlantic Bight and over Georges Bank. *Mar.*
1136 *Ecol. Prog. Ser.* 380, 147-160
1137 Tremblay, M. J. 1988. A summary of the proceedings of the Halifax sea scallop
1138 workshop, August 13-14, 1987. Canadian Technical Report of Fisheries and
1139 Aquatic Sciences, No. 1605, 12 pp.
1140 Tremblay, M. J., Sinclair, M., 1990a. Sea scallop larvae Placopecten magellanicus on
1141 Georges Bank: Vertical distribution in relation to water column stratification and
1142 food. Marine Ecology Progress Series 61(1-2):1-15, doi: 10.3354/meps061001
1143 Tremblay, M. J. Sinclair,M., 1990b. Diel migration of sea scallop larvae Placopecten
1144 magellanicus in a shallow embayment. Marine Ecology Progress Series 67, 19-25.
1145 Tremblay, M. J., Loder, J. W., Werner, F. E., Naimie, C. E., Page, F. H., and Sinclair, M.
1146 M. 1994. Drift of sea scallop larvae Placopecten magellanicus on Georges Bank: a
1147 model study of the roles of mean advection, larval behavior and larval origin.
1148 *Deep-Sea Research* II, 41: 7–49.
1149 Van Sebille, E., Van Leeuwen, P. J., Biastoch, A., Barron, C. N., Ruijter, D., 2009.
1150 Lagrangian validation of numerical drifter trajectories using drifting buoys:
1151 Application to the Agulhas system. *Ocean Modelling* 29, 269-276.
1152 Werner, F. E., Page, F. H., Lynch D. R., Loder J. W. and others, 1993. Influence of mean
1153 3-D advection and simple behavior on the distribution of cod and haddock early
1154 life stages on Georges Bank. Fish Oceanogr. 2: 43-64.
1155 Woods, J., 2005. The Lagrangian ensemble metamodel for simulating plankton systems.
1156 Progress in Oceanography 67: 84–159

Zhang, Y., Chen, C., Beardsley, R. C., Gao, G., Lai, Z., Curry, B., Lee, C. M., Lin, H., Qi, J., Xu, Q., 2016. Studies of the Canadian Arctic Archipelago water transport and its relationship to basin-local forcings: Results from AO-FVCOM. *Journal of Geophysical Research-Oceans* 121, doi:10.1002/2016JC011634., 121.

Zhang, Y., Chen, C., Beardsley, R. C., Gao, G., Qi, J., Lin, H., 2016. Seasonal and interannual variability of the Arctic sea ice: a comparison between AO-FVCOM and observations. *Journal of Geophysical Research-Ocean*s 121, doi: 10.1002/ 2016JC011841.

Figure Captions

Figure 1: Schematic of the near-surface (red arrows) and deep (white arrows) flows over the US northeast shelf. GB: Georges Bank, GSC: Great South Channel, SNE: Southern New England, MAB: Middle Atlantic Bight. The red color patch represents the Gulf Stream northward meander water. Red color rings represent the warm-core ring separated from the Gulf Stream. Gray thick lines are the boundaries between GB/GSC, SNE, and MAB. The solid black thin line is the transect where the transport was calculated. The 3-D icon represents the NOAA buoy, and the number on the right is the buoy number.

Figure 2: The unstructured meshes for Global-FVCOM and GoM-FVCOM. The cells marked with red colors represent the common cells nesting between Global-FVCOM and GoM-FVCOM.

Figure 3: Structures of the scallop-IBM early life stage model. Four pelagic stages are considered: 1) egg, 2) trochophore, 3) veliger, and 4) pediveliger. U, V, and W are the x, y, and z components of the water velocity. T is the water temperature, and K_m is the vertical eddy viscosity. The dashed line box presents the pelagic stages, and the gray shadow area indicates benthic stages.

Figure 4: The diel and semidiurnal larval vertical migration sub-models in the surface mixed layer during the period of 5 through 40 days from eggs to veliger stages. Diel and semi-diurnal vertical migration patterns were based on the observations made by *Tremblay and Sincl*air (1990b), *Manuel et al*. (1996), and *Gallager et al*.

(1996). The number in the figure indicates the time of a day defined by a 24-hour clock.

Figure 5: Scallop abundance (scallop#/m^2) (a) and gridded density (individual/m^2) (b) for spawning The individuals in each cell were determined using the combined scallop data from BIO, NOAA, and SMAST. In the upper panel, shapes bounded by red lines are the closed areas; CA-I: closed area I, CA-II: closed area II, and NLCA: Nantucket Lightship closed area. In the lower panel, the dashed thick line is the boundary between the US and Canadian waters.

Figure 6: Illustration of the egg spawning period starting at 00:00 September 1 and ending at 24:00 October 10. The spawning process satisfies a normal probability distribution with the maximum on September 20 and a one-week standard deviation.

Figure 7: Distributions of the settled larval density (a-e) and locations/ abundances of settled super-individuals (f-j) for the cases C#1 (No OML), C#2 (10 m-OML: diel), C#3 (10 m-OML: semidiurnal), C#4 (30 m-OML: diel), and C#5 (30 m-OML: semidiurnal). The results were from the 2008 simulation. Two thick gray lines are the boundaries between GB/GSC, SNE, and MAB. Gray lines with labels are 50, 100, and 200-m isobath contours.

Figure 8: Distributions of the settled larval density (a-e) and locations/ abundances of settled super-individuals (f-j) for the cases C#1 (No OML), C#2 (10 m-OML: diel), C#3 (10 m-OML: semidiurnal), C#4 (30 m-OML: diel), and C#5 (30 m-OML: semidiurnal). The results were from the 2009 simulation. Two thick gray lines are the boundaries between GB/GSC, SNE, and MAB. Gray lines with labels are 50, 100, and 200-m isobath contours.

Figure 9: Distributions of the settled larval density (a-e) and locations/ abundances of settled super-individuals (f-j) for the cases C#1 (No OML), C#2 (10 m-OML: diel), C#3 (10 m-OML: semidiurnal), C#4 (30 m-OML: diel), and C#5 (30 m-OML: semidiurnal). The results were from the 2012 simulation. Two thick gray lines are the boundaries between GB/GSC, SNE, and MAB. Gray lines with labels are 50, 100, and 200-m isobath contours.

Figure 10: Distributions of the settled larval density (a-e) and locations/ abundances of

1219 settled super-individuals (f-j) for the cases C#1 (No OML), C#2 (10 m-OML:
1220 diel), C#3 (10 m-OML: semidiurnal), C#4 (30 m-OML: diel), and C#5 (30 m-
1221 OML: semidiurnal). The results were from the 2013 simulation. Two thick gray
1222 lines are the boundaries between GB/GSC, SNE, and MAB. Gray lines with
1223 labels are 50, 100, and 200-m isobath contours.
1224 Figure 11: Ratio of the model-simulated mixed layer to the local depth averaging over
1225 September-November, 2013. The right lower panel shows the cross-isobath
1226 distributions of temperature and salinity on GB. The solid black thick line is the
1227 location of the section. Black lines are 50, 100, and 200-m isobath contours.
1228 Figure 12: Cross-isobath sections (thick white lines) labeled "A, B, and C" and the depths
1229 of the monthly averaged OML for September, October, and November 2013 on
1230 Sections A, B, and C, respectively. Red line: September, blueline: October, and
1231 blackline: November. Black lines are the isobath contours matching with depth
1232 images.
1233 Figure 13: Distributions of the settled larval density (a-c) and locations/ abundances of
1234 settled super-individuals (d-f) for the cases C#6 (varying OML: diel), C#7
1235 (varying OML: semidiurnal), and C#8 (thermocline-migration). The results were
1236 from the 2013 simulation. Two thick gray lines are the boundaries between
1237 GB/GSC, SNE, and MAB. Gray lines with labels are the 50, 100, and 200-m
1238 isobath contours.
1239 Figure 14: Horizontal and vertical trajectories of a super-individual originating from the
1240 same site on the southeastern flank of GB. a: C#1 (No OML); b: C#2 and C#3 (10
1241 m-OML); c: C#4 and C#5 (30 m-OML); d: C#6, C#7, and C#8 (Varying OML). t_d:
1242 diel; t_{sd}: semidiurnal; m_b: thermocline-seeking. The results were from the 2013
1243 simulation. Black lines are the isobath contours matching with depth images.
1244 Figure 15: The 39-year mean, percentage, and standard deviation of settled scallop larvae
1245 over 1978-2016 for C#1-C#5. a-c: C#1 (No OML); d-f: C#2 (10 m-OML: diel); g-
1246 i: C#3 (10 m-OML: semidiurnal); j-l: C#4 (30 m-OML: diel); m-o: C#5 (30 m-
1247 OML: semidiurnal). Two thick gray lines are the boundaries between GB/GSC,
1248 SNE, and MAB. Gray lines are the 50, 100, and 200-m isobath contours (see Fig.
1249 11 for isobath labels).

Figure 16: Model-predicted percentages of the scallop larvae settling in the GB/GSC (a), SNE (b), and MAB (c) regions, respectively, over 1978-2016 for C#1 (solid black line), C#2 (solid blue line), C#3 (dashed blue line), C#4 (solid red line), and C#5 (dashed red line).

Figure 17: The 4-year mean, percentage, and standard deviation of settled scallop larvae over 2013-2016 for C#6, C#7, and C#8. a-c: C#6 (varying OML: diel); d-f: C#7 (varying OML: semidiurnal); g-i: C#8 (thermocline-migration). Two thick gray lines are the boundaries between GB/GSC, SNE, and MAB. Gray lines are the 50, 100, and 200-m isobath contours (see Fig. 11 for isobath labels).

Figure 18: Model-predicted percentages of the scallop larvae settling in the GB/GSC (a) and SNE (b) regions, respectively, over 2013-2016 for the cases C#4 (30 m-OML: diel), C#5 (30 m-OML: semidiurnal), C#6 (varying OML: diel), C#7 (varying OML: semidiurnal), and C#8 (thermocline-migration).

Figure 19: Distributions of the three-monthly averaged bottom temperature in the region covering GB, SNE, and the MAB over September-November. a: 1978-2008-averaged; b: 2009; c: 2012; d: 2013-2016 averaged.

Figure 20: b: distribution of the yearly surface temperature increase rate calculated based on the satellite-derived SST data over 1982-2020. The temperature increase rate was estimated based on the annual increase rate calculating over two consecutive years. a: the change of the satellite-derived SST over the shelf bounded by the 300-m isobath over 1982-2019. Solid black dots: the yearly averaged SST for each year; thick red line: the linear regression fitting line; thick blue dashed lines: averaged SSTs over 1982-2011 and 2012-2020, respectively.

Figure 21: Anomalies of the water transport through an across-shelf section over the SNE shelf (see the location in Figure 1) over 1978-2016. The value listed in the upper-right area is the 39-year mean water transport.

Figure 22: The wind rose plot at NOAA buoy 44008 for September-November, 2009.

Figure A1: Illustration of the density profile under a vertically well-mixed condition for Case 1.

Figure A2: Illustration of a linear density profile under a stratified condition for Case 2.

Figure A3: Illustration of a two-layer system in which the water density is constant in the

upper layer and linearly increases with depth in the lower layer for Case 3.

Figure A4: Vertical profiles of sea temperature (red), salinity (blue), and density (black) at three sites across GB at 00:00 GMT, September 1, 2013. The thick dashed line represents the OML depth calculated using Eq. A.1 in Appendix A.

Table 1: Types of numerical experiments made in this study

Parameters / Case	OML	Larva behavior
Case 1 (C#1)	No	No
Case 2 (C#2)	10 m	diel migration
Case 3 (C#3)	10 m	semidiurnal migration
Case 4 (C#4)	30 m	diel migration
Case 5 (C#5)	30 m	semidiurnal migration
Case 6 (C#6)	varying	diel migration
Case 7 (C#7)	varying	semidiurnal migration
Case 8 (C#8)	varying	thermocline-seeking

Table 2: Mean percentages and standard deviations of larvae settling in GB/GSC, SNE, and MAB over 1978-2016 for C#1-C#5.

Zone / Case	GB/GSC	SNE	MAB
C#1: No OML	43.7±12.4	34.2±12.5	22.1±13.9
C#2: 10-m OML: diel	50.7±6.5	41.1±6.3	8.2±6.3
C#3: 10-m OML: semidiurnal	53.9±7.5	39.8±5.8	6.3±4.9
C#4; 30-m OML: diel	40.7±7.0	57.5±6.6	1.8±2.7
C#5: 30-m OML: semidiurnal	46.3±7.2	53.0±7.5	0.7±2.8

Table 3: Mean percentages and standard deviations of larvae settling in GB/GSC, SNE, and MAB over 2013-2016 for C#6, C#7, and C#8.

Zone / Case	GB/GSC	SNE	MAB
C#6: Varying OML: diel	53.5±7.0	46.5±7.1	0.0±0.1
C#7: Varying OML: semidiurnal	57.7±6.1	42.5±6.1	0.0±0.0
C#8: Varying OML: thermocline-seeking	62.9±8.8	37.1±8.8	0.0±0.0

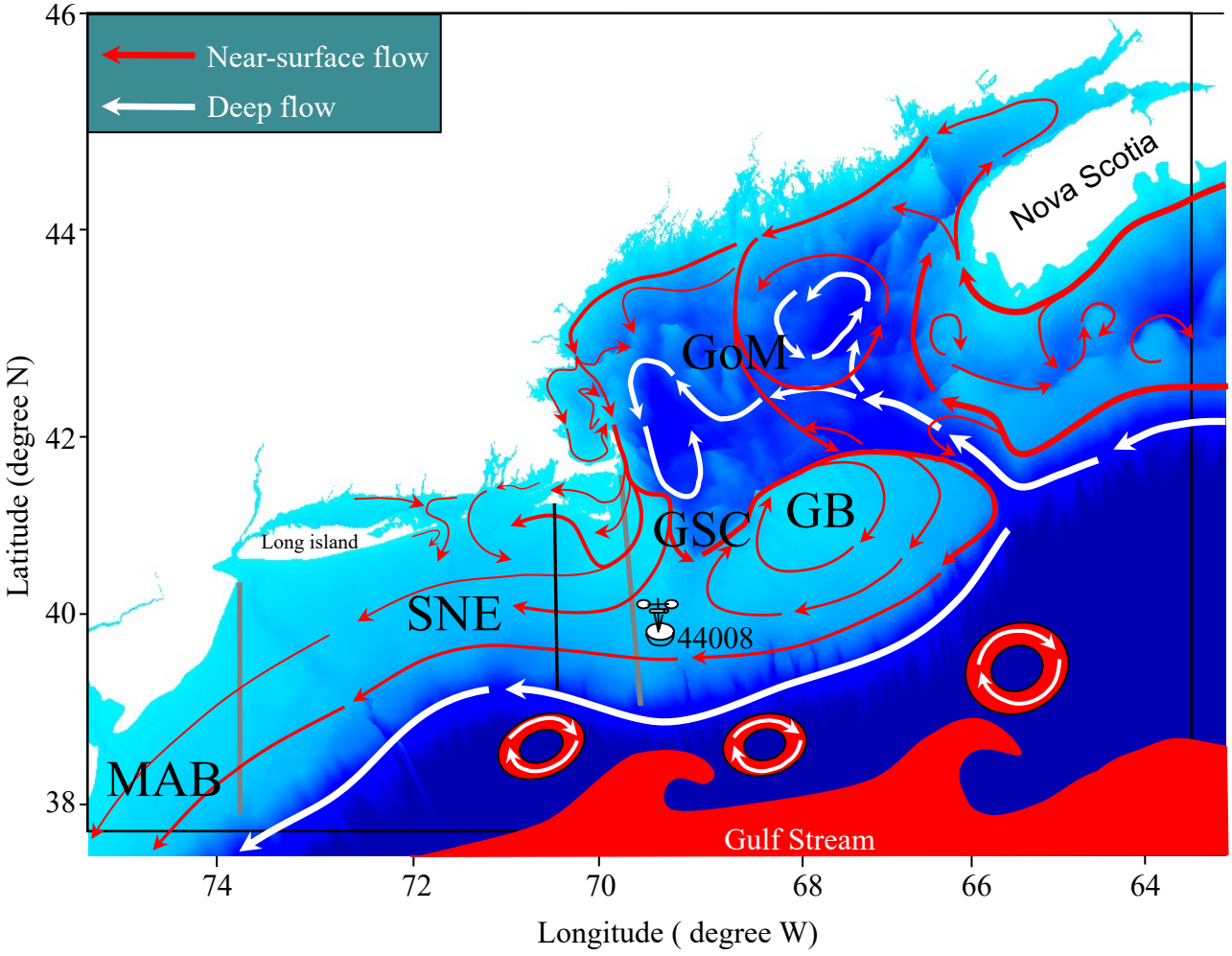
Near-surface flow
Deep flow
Nova Scotia
GoM
GSC
GB
Long island
SNE
44008
MAB
Gulf Stream
46
44
42
40
38
74
72
70
68
66
64
Latitude (degree N)
Longitude (degree W)

Figure 1

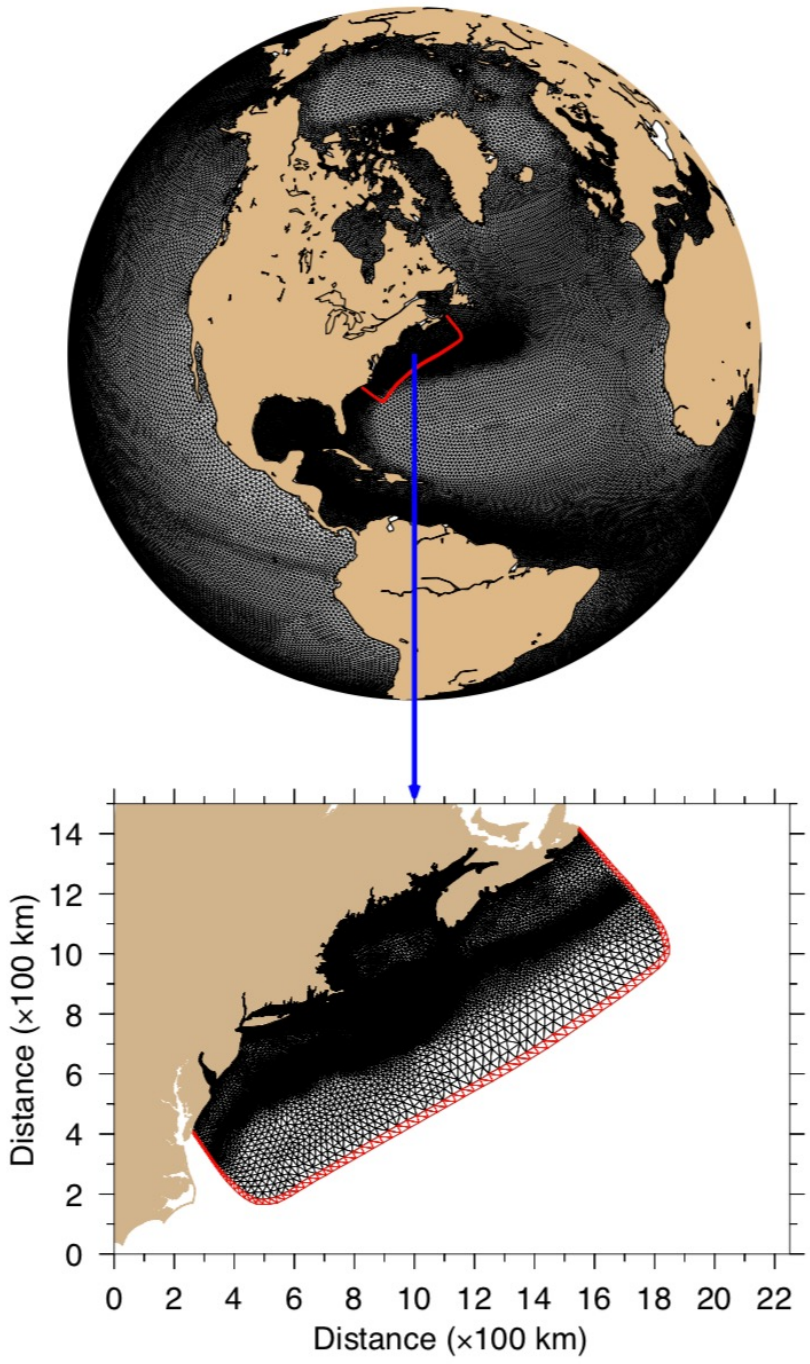
Distance (×100 km)
0
2
4
6
8
10
12
14
Distance (×100 km)
0
2
4
6
8
10
12
14
16
18
20
22

Figure 2

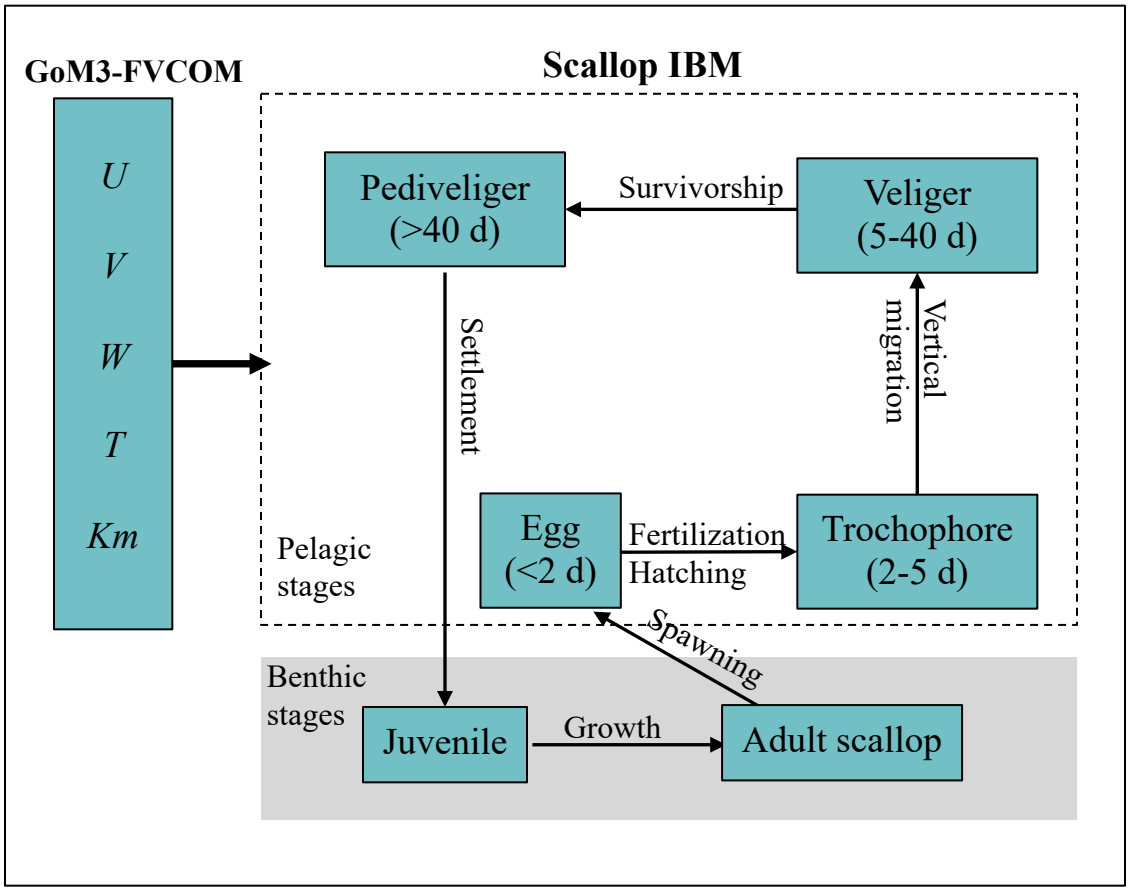
GoM3-FVCOM
Scallop IBM
U
V
W
T
Km
Pediveliger
(>40 d)
Survivorship
Veliger
(5-40 d)
Settlement
Vertical
migration
Egg
(<2 d)
Fertilization
Hatching
Trochophore
(2-5 d)
Pelagic
stages
Spawning
Benthic
stages
Juvenile
Growth
Adult scallop

Figure 3

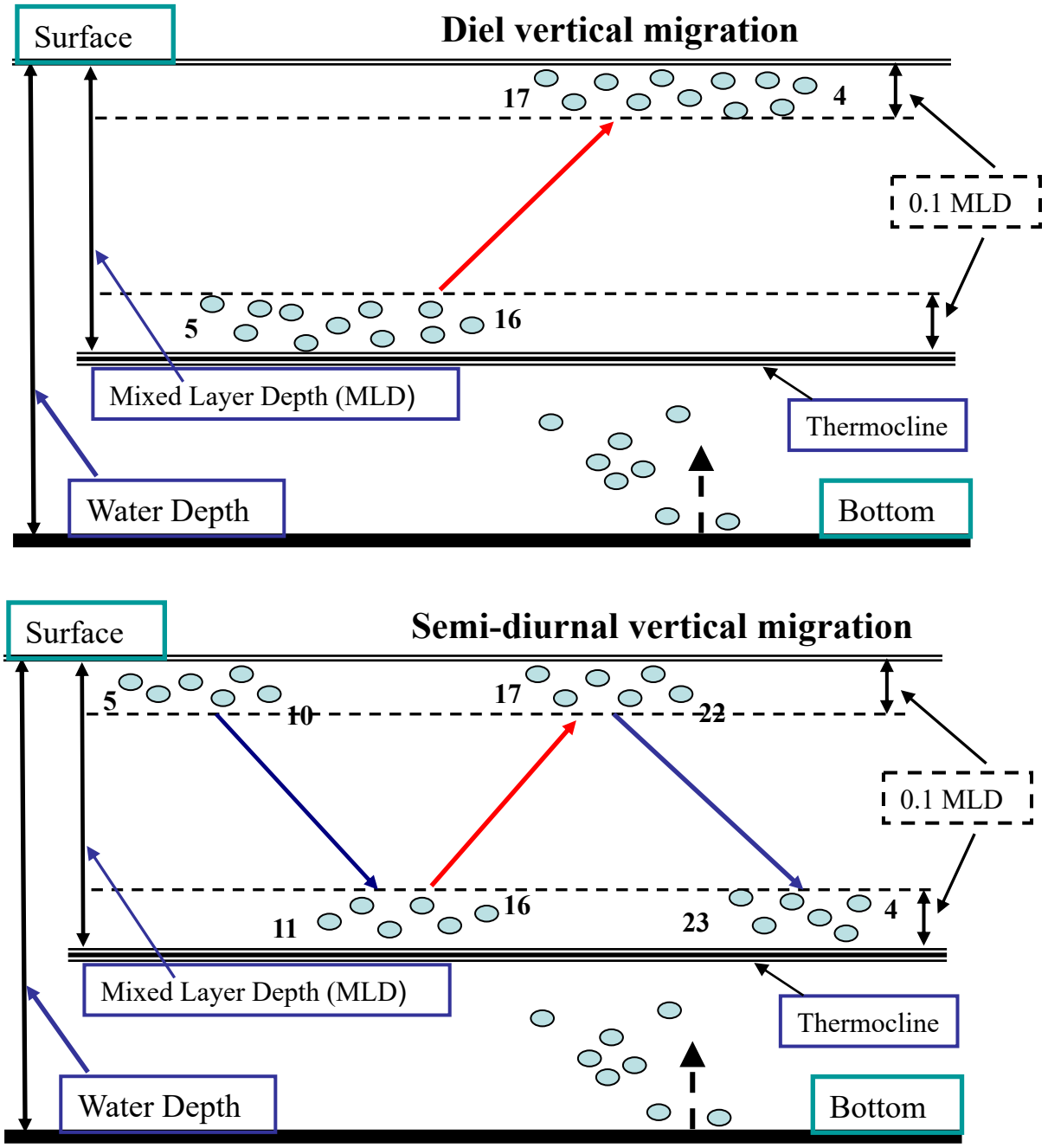
Surface
Diel vertical migration
17
4
0.1 MLD
5
16
Mixed Layer Depth (MLD)
Thermocline
Water Depth
Bottom
Surface
Semi-diurnal vertical migration
5
10
17
22
0.1 MLD
11
16
23
4
Mixed Layer Depth (MLD)
Thermocline
Water Depth
Bottom

Figure 4

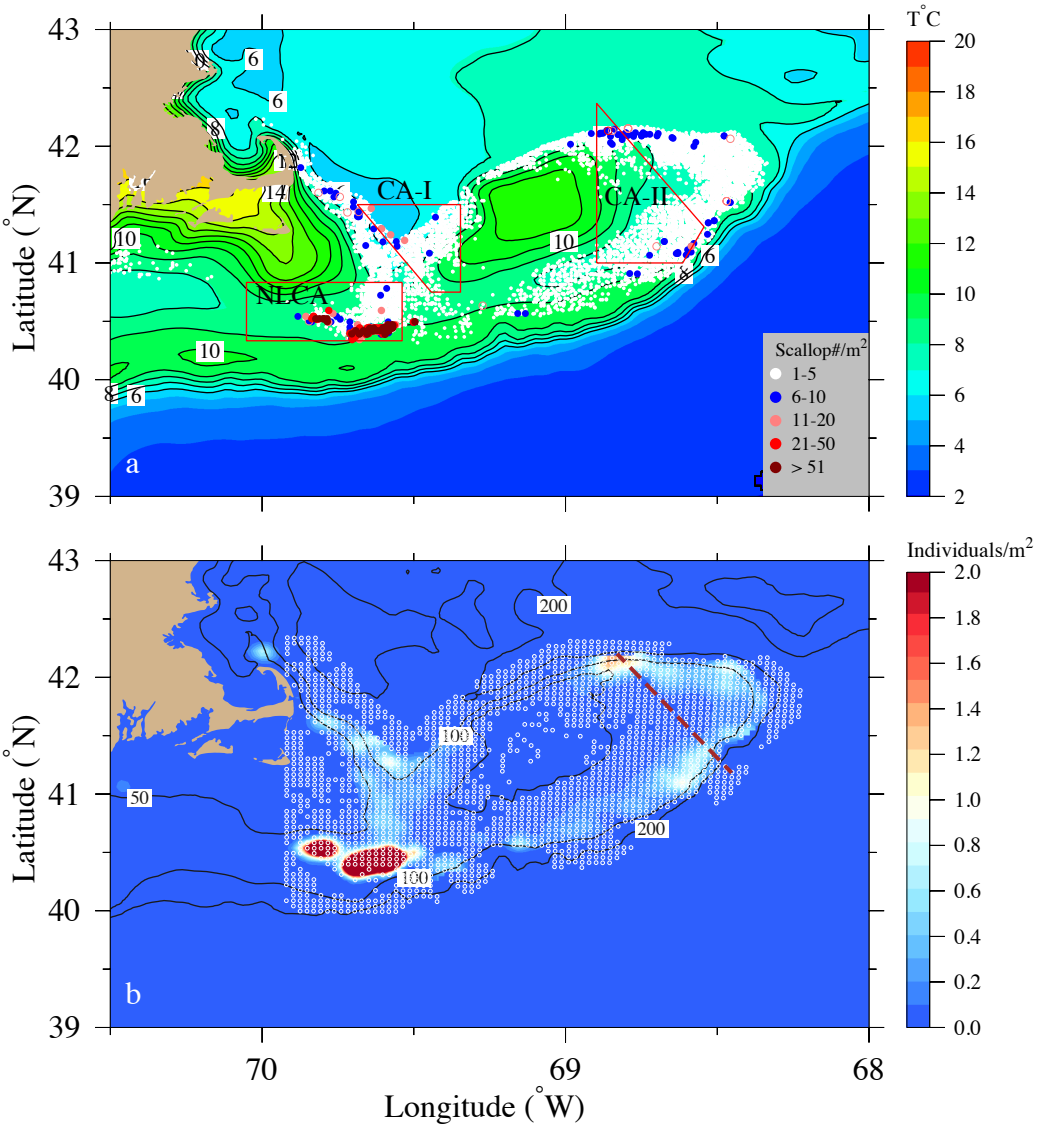
43
42
41
40
39
Latitude (°N)
6
8
10
12
14
CA-I
CA-II
NLCA
a
Scallop#/m2
1-5
6-10
11-20
21-50
> 51
T°C
20
18
16
14
12
10
8
6
4
2
Individuals/m2
2.0
1.8
1.6
1.4
1.2
1.0
0.8
0.6
0.4
0.2
0.0
50
100
200
b
70
69
68
Longitude (°W)

Figure 5

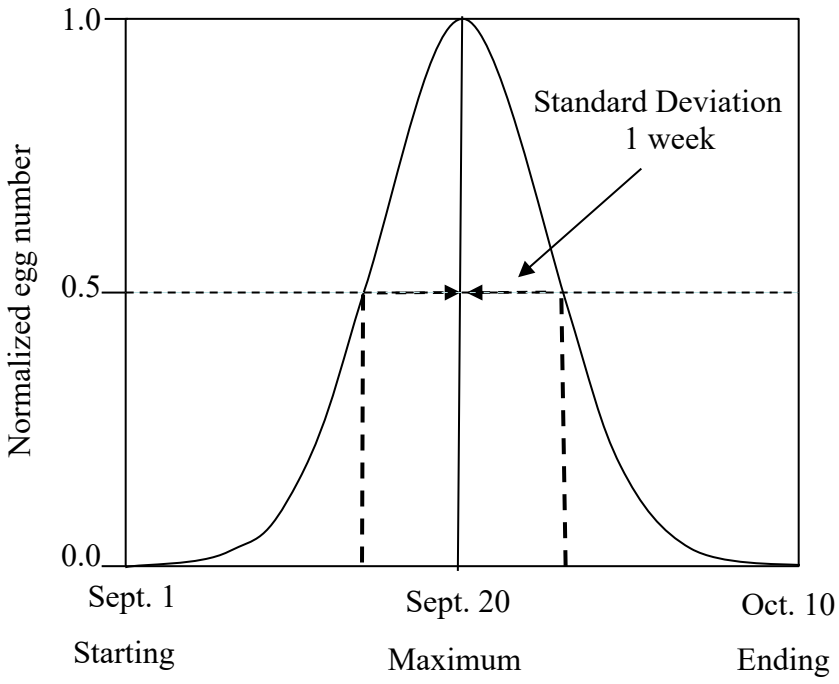
1.0
0.5
0.0
Normalized egg number
Standard Deviation
1 week
Sept. 1
Starting
Sept. 20
Maximum
Oct. 10
Ending

Figure 6

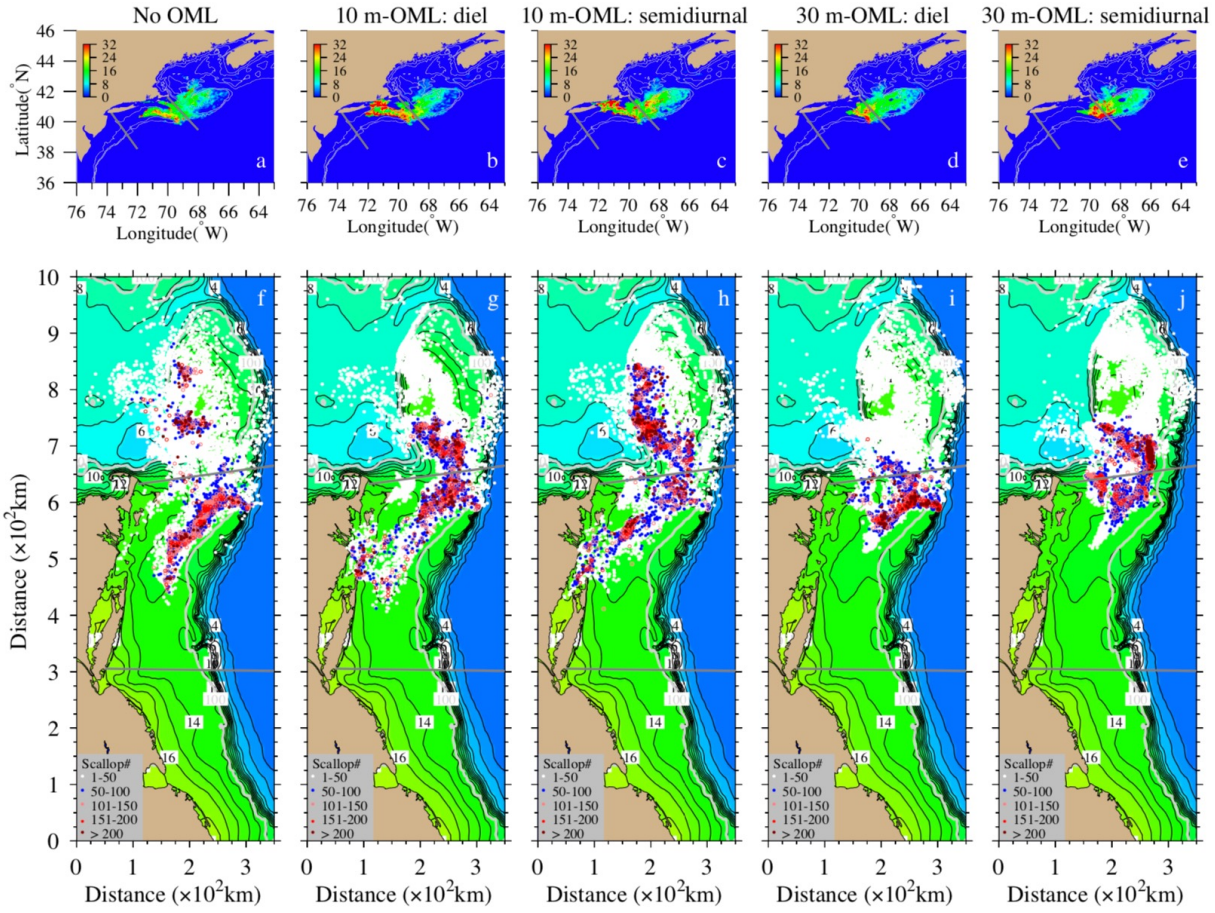
No OML
10 m-OML: diel
10 m-OML: semidiurnal
30 m-OML: diel
30 m-OML: semidiurnal
Latitude(°N)
Longitude(°W)
Distance (×10²km)
Scallop#
1-50
50-100
101-150
151-200
> 200
a
b
c
d
e
f
g
h
i
j

Figure 7

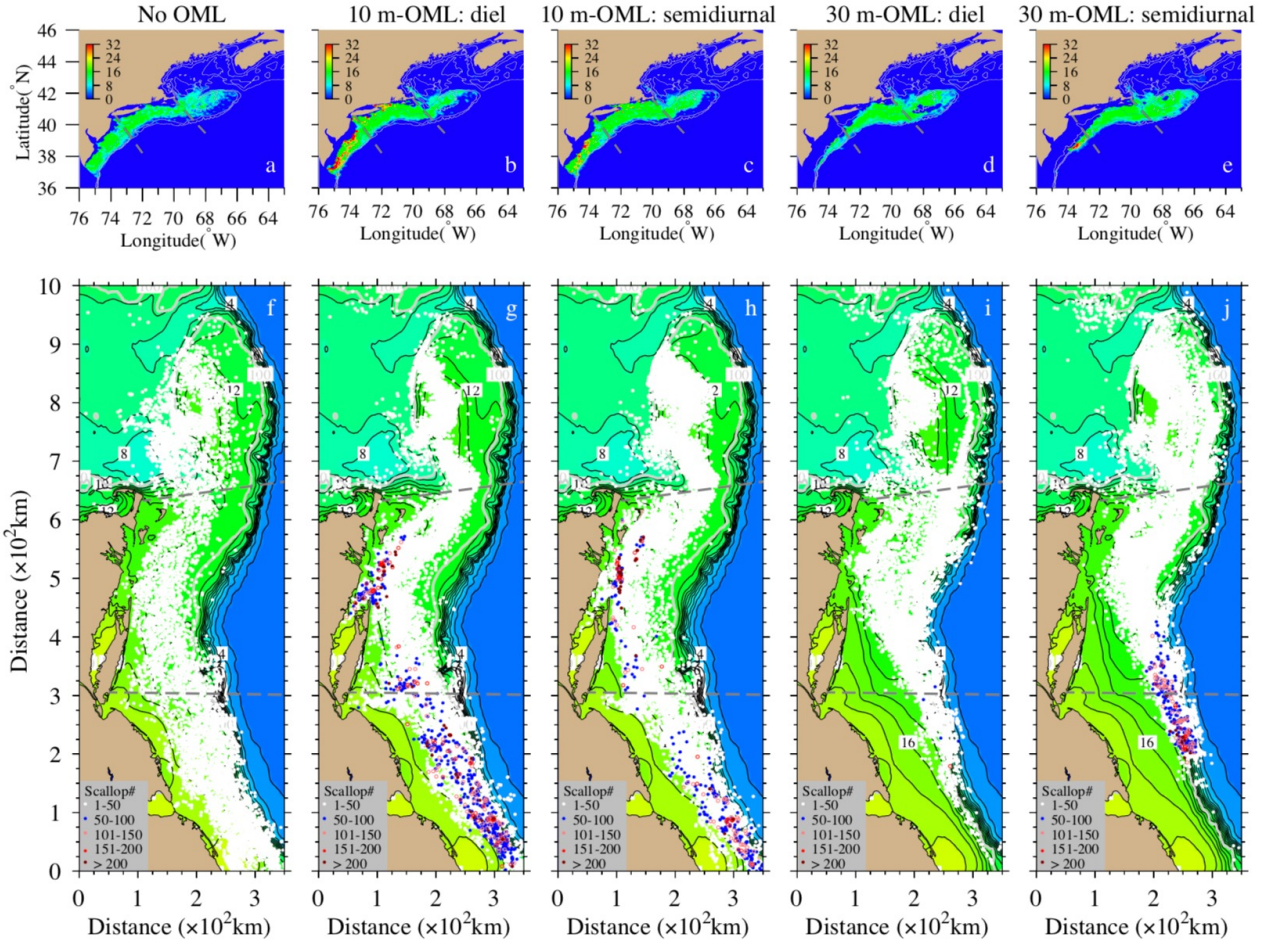
No OML
10 m-OML: diel
10 m-OML: semidiurnal
30 m-OML: diel
30 m-OML: semidiurnal
Latitude(°N)
Longitude(°W)
Distance (×10²km)
Scallop#
1-50
50-100
101-150
151-200
> 200
a
b
c
d
e
f
g
h
i
j

Figure 8

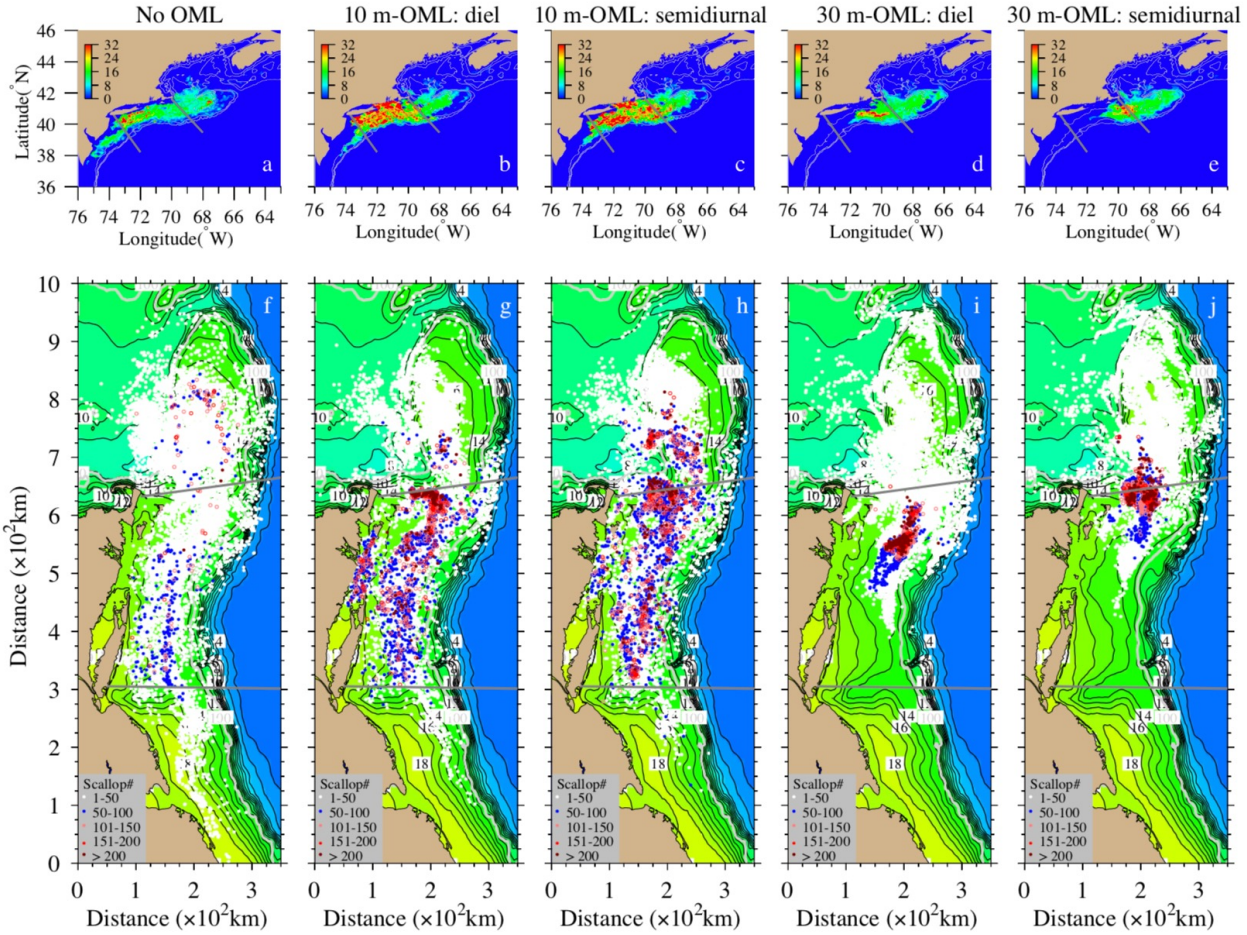
No OML
10 m-OML: diel
10 m-OML: semidiurnal
30 m-OML: diel
30 m-OML: semidiurnal
Latitude(°N)
Longitude(°W)
Distance (×10²km)
Scallop#
1-50
50-100
101-150
151-200
> 200

Figure 9

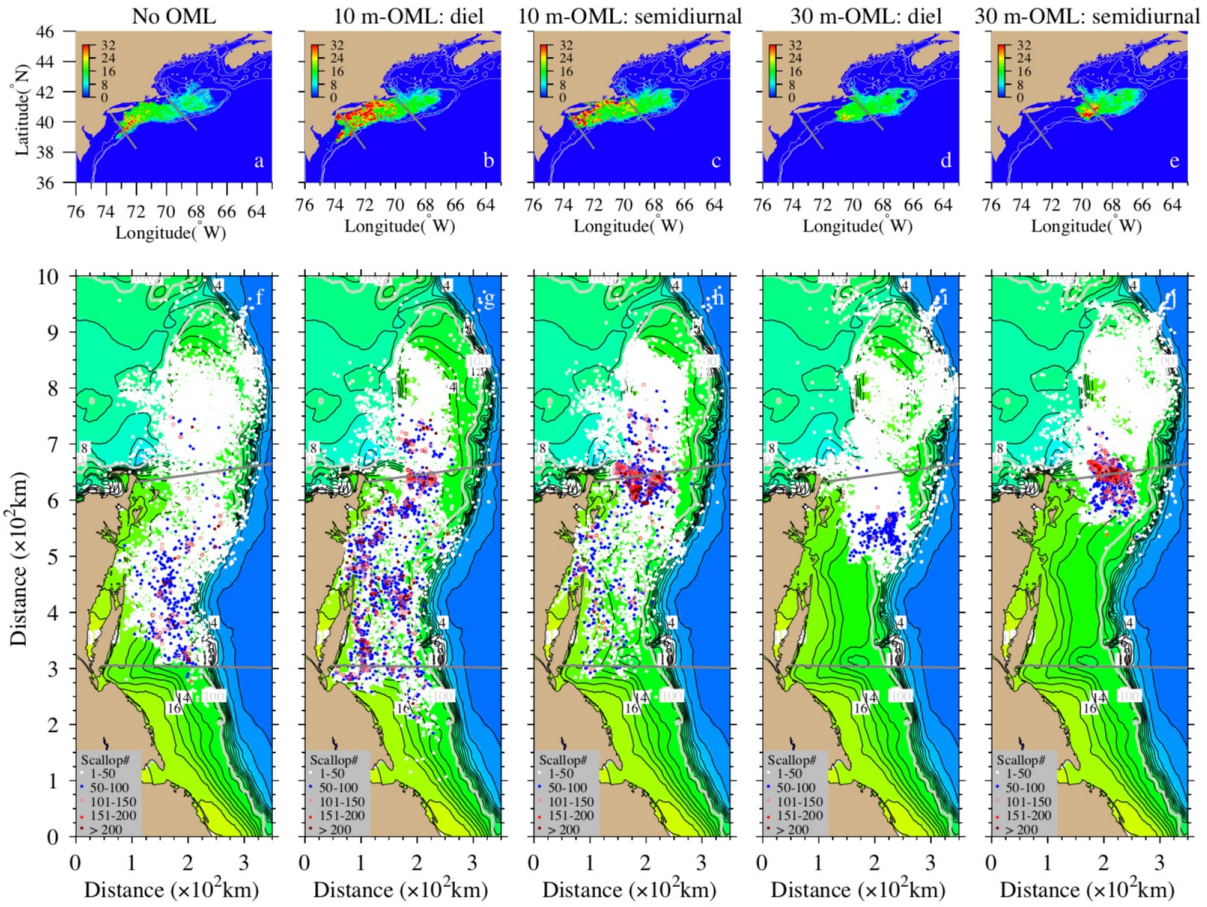
No OML
10 m-OML: diel
10 m-OML: semidiurnal
30 m-OML: diel
30 m-OML: semidiurnal
Latitude(°N)
Longitude(°W)
Distance (×10²km)
Scallop#
1-50
50-100
101-150
151-200
> 200

Figure 10

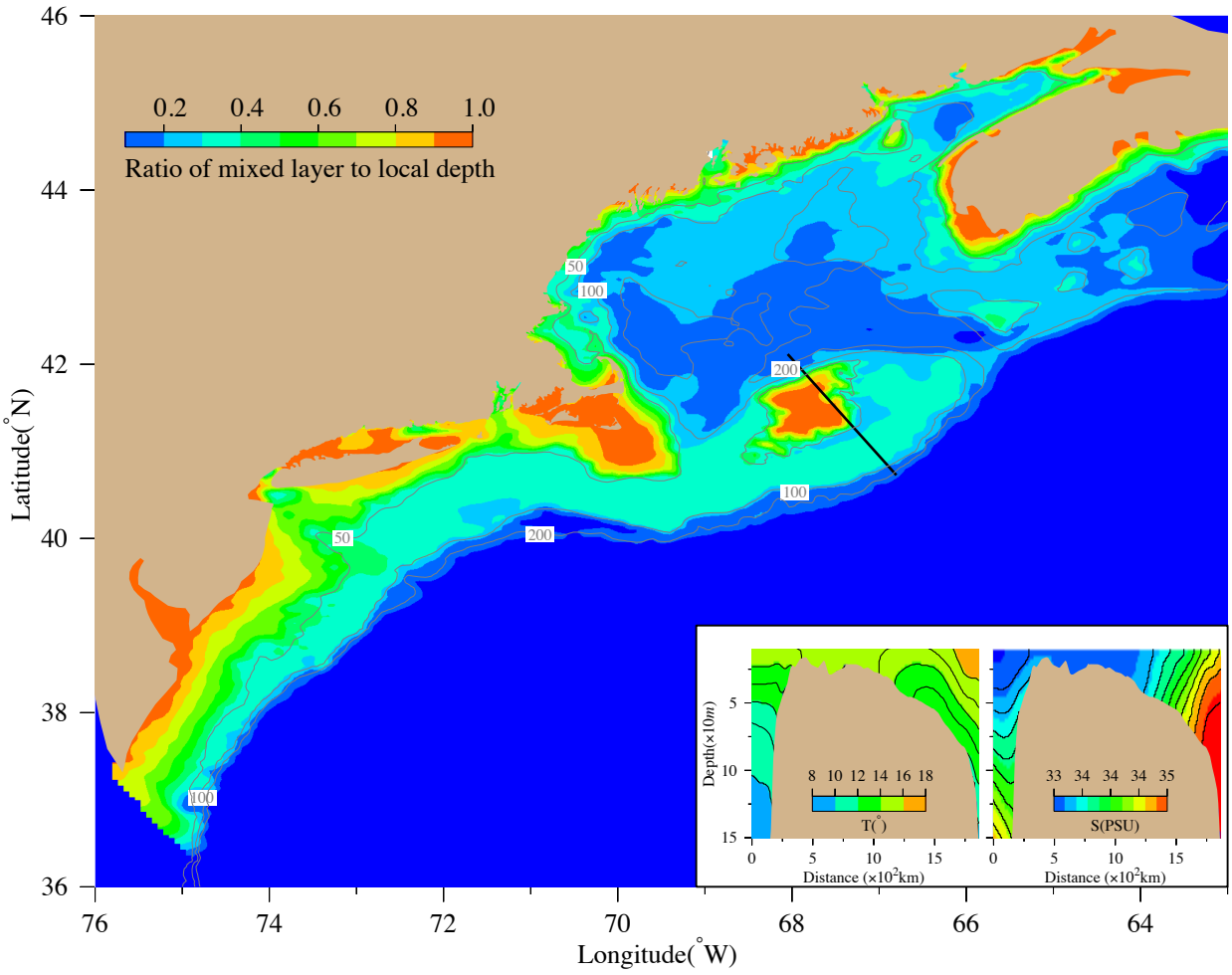
0.2 0.4 0.6 0.8 1.0
Ratio of mixed layer to local depth
50
100
200
100
50
200
100
46
44
42
40
38
36
Latitude(°N)
76
74
72
70
68
66
64
Longitude(°W)
Depth(×10m)
5
10
15
8 10 12 14 16 18
T(°)
33 34 34 34 35
S(PSU)
0 5 10 15
Distance (×10²km)
0 5 10 15
Distance (×10²km)

Figure 11

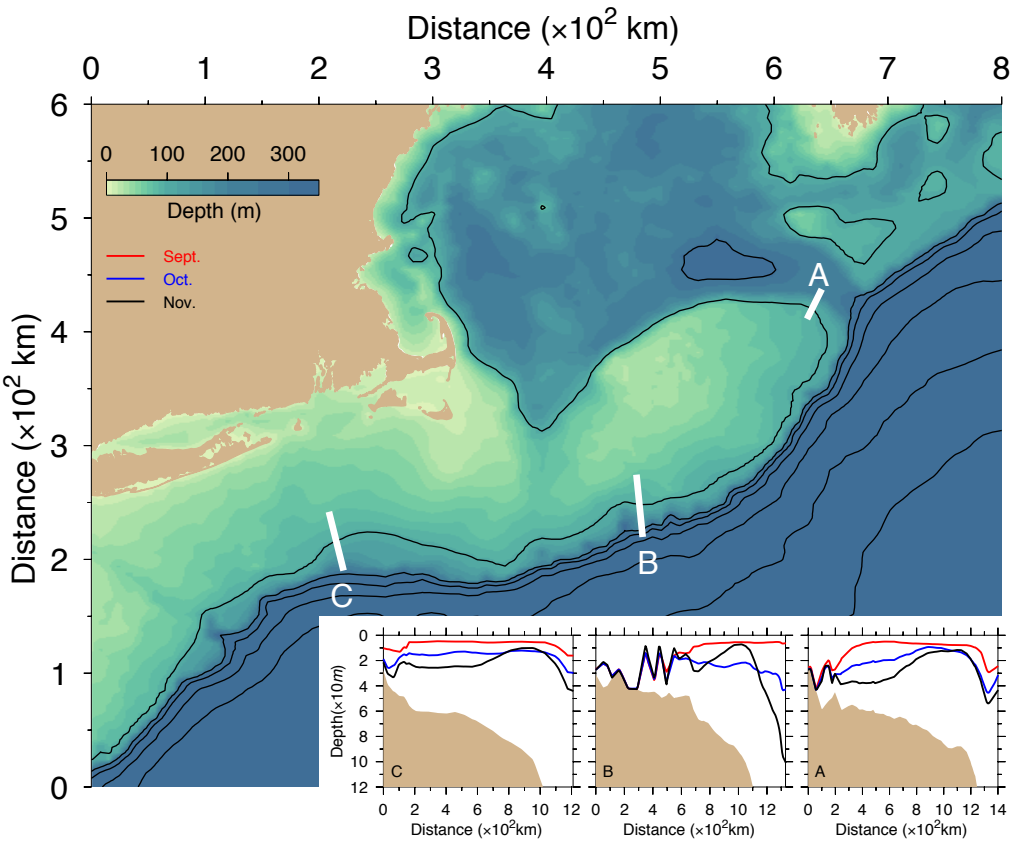
Distance (×10² km)
0 1 2 3 4 5 6 7 8
Distance (×10² km)
0 1 2 3 4 5 6
0 100 200 300
Depth (m)
Sept.
Oct.
Nov.
A
B
C
Depth(×10m)
0 2 4 6 8 10 12
C
0 2 4 6 8 10 12
Distance (×10²km)
B
0 2 4 6 8 10 12
Distance (×10²km)
A
0 2 4 6 8 10 12 14
Distance (×10²km)

Figure 12

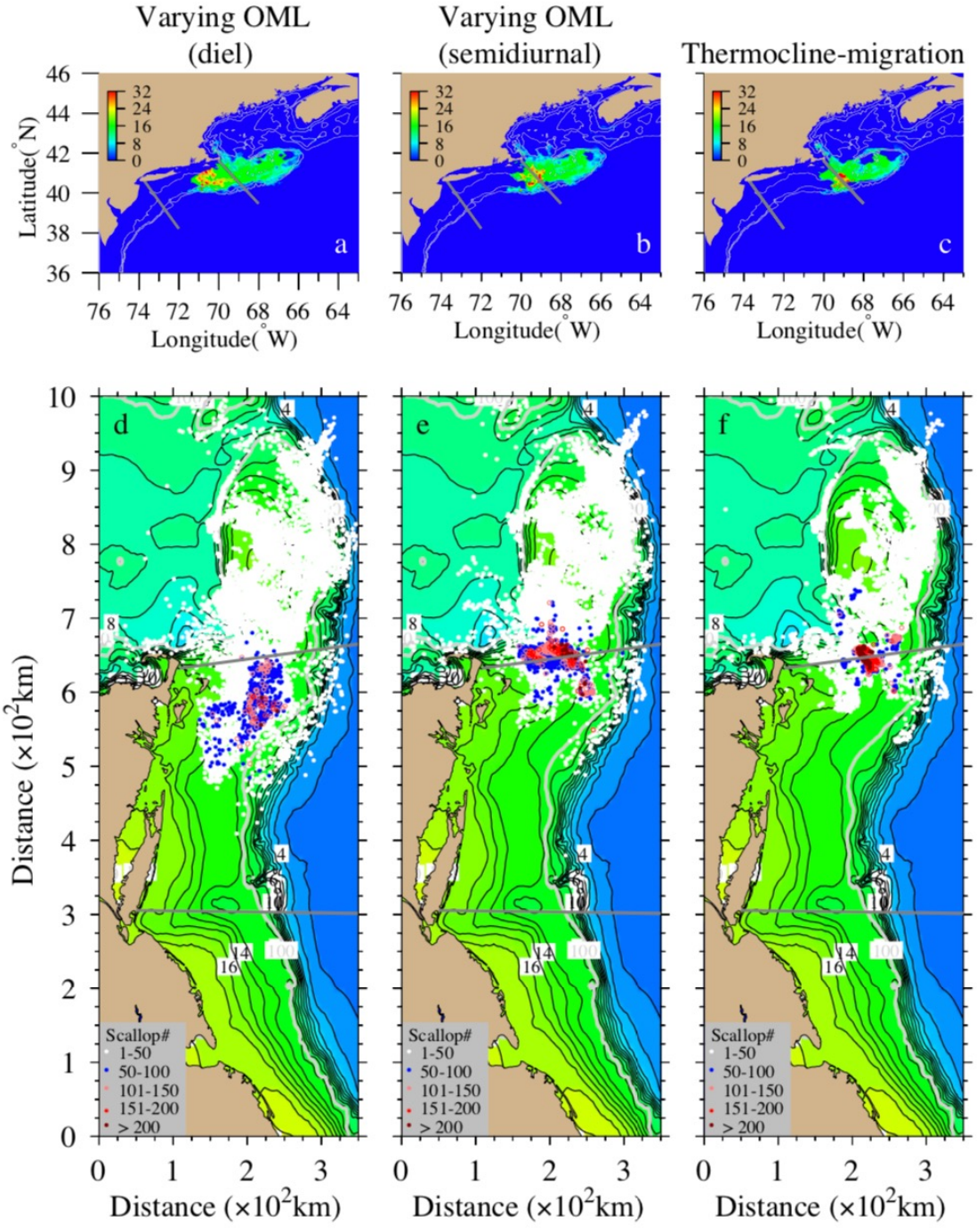
Varying OML
(diel)
Varying OML
(semidiurnal)
Thermocline-migration
Latitude(°N)
Longitude(°W)
a
b
c
d
e
f
Distance (×10²km)
Scallop#
1-50
50-100
101-150
151-200
> 200

Figure 13

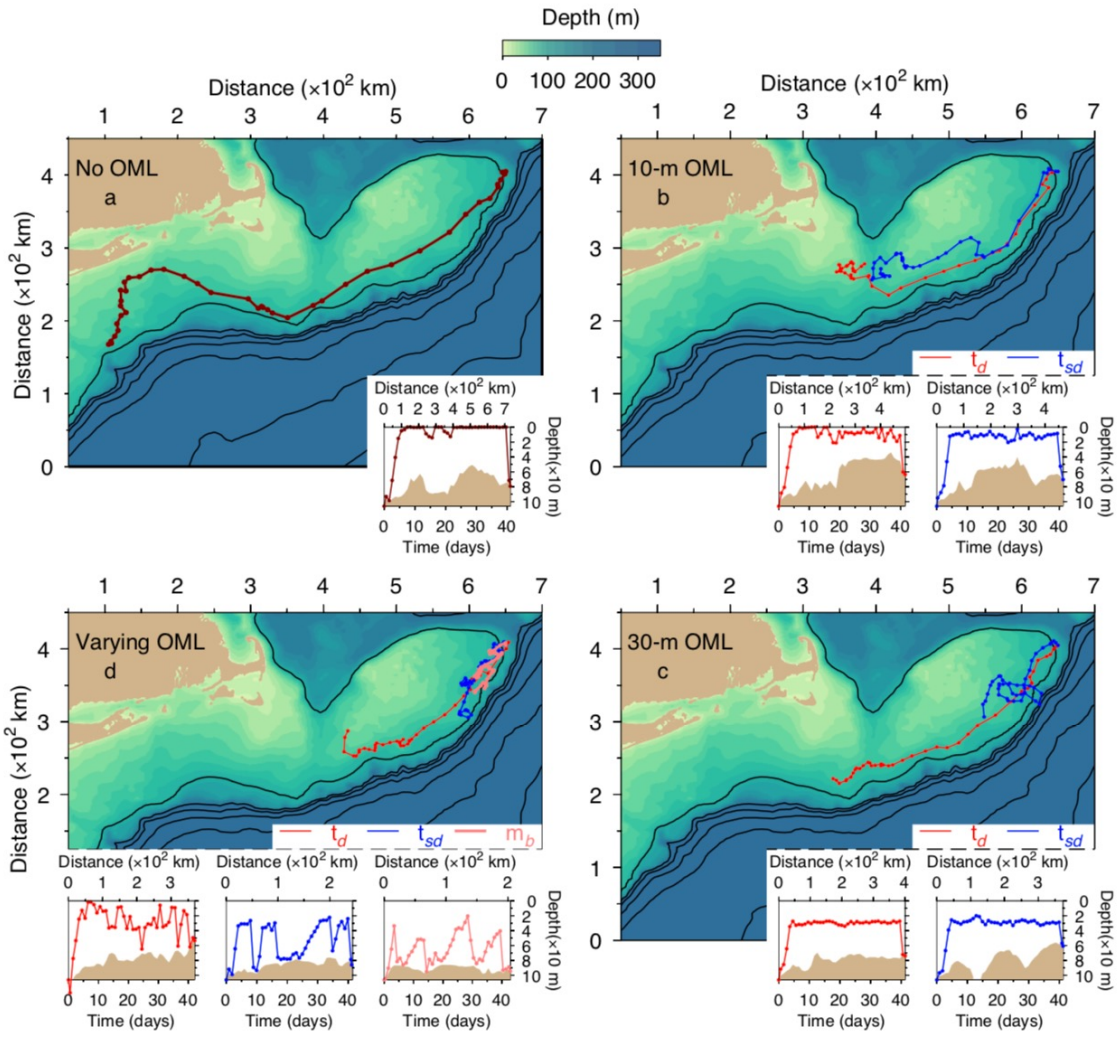
Depth (m)
0 100 200 300
Distance (×10² km)
No OML
a
10-m OML
b
Varying OML
d
30-m OML
c
Distance (×10² km)
Time (days)
Depth(×10 m)
t_d
t_sd
m_b

Figure 14

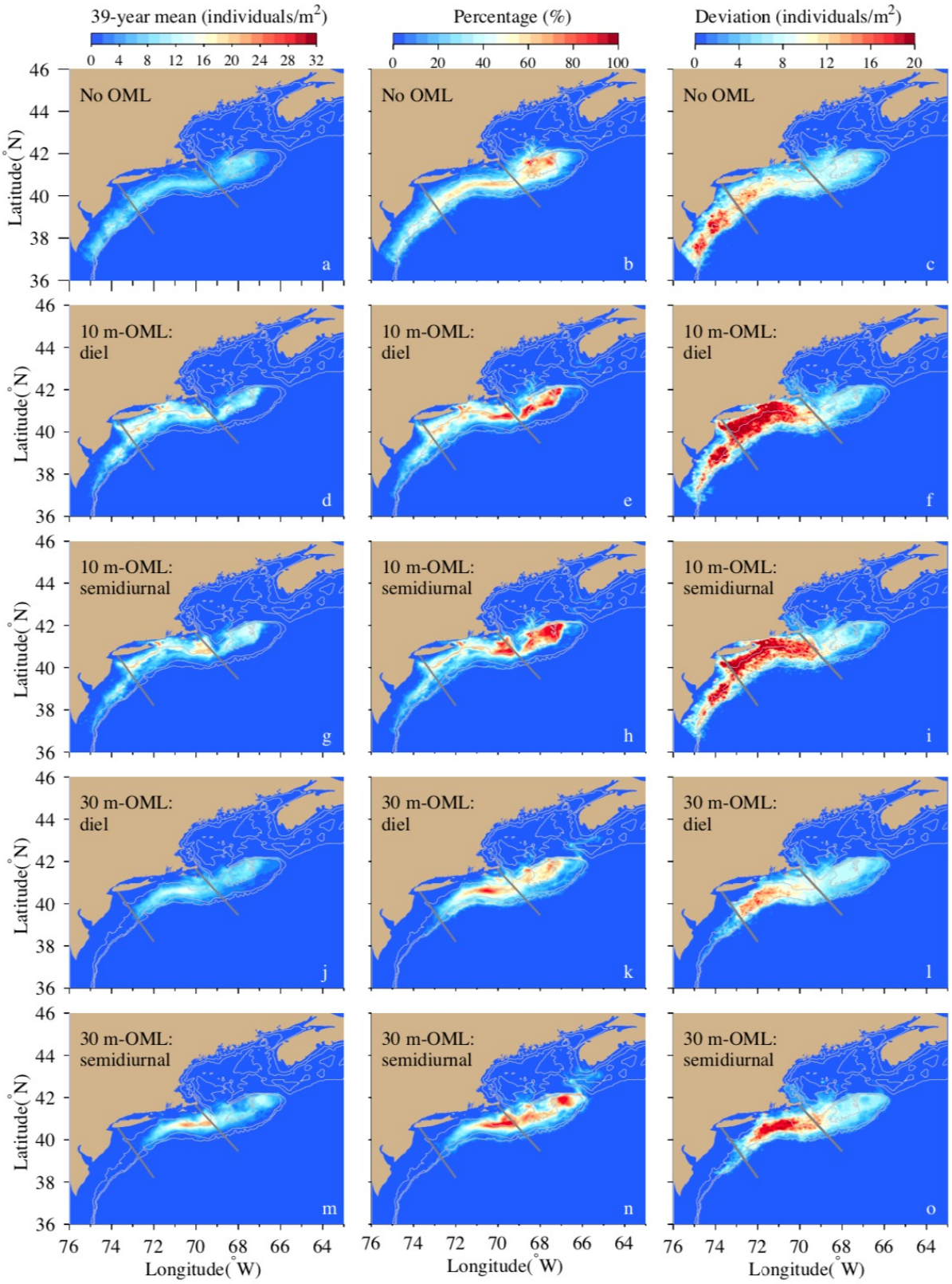
39-year mean (individuals/m^2)
0 4 8 12 16 20 24 28 32
Percentage (%)
0 20 40 60 80 100
Deviation (individuals/m^2)
0 4 8 12 16 20
No OML
a
No OML
b
No OML
c
10 m-OML: diel
d
10 m-OML: diel
e
10 m-OML: diel
f
10 m-OML: semidiurnal
g
10 m-OML: semidiurnal
h
10 m-OML: semidiurnal
i
30 m-OML: diel
j
30 m-OML: diel
k
30 m-OML: diel
l
30 m-OML: semidiurnal
m
30 m-OML: semidiurnal
n
30 m-OML: semidiurnal
o
Latitude(°N)
46 44 42 40 38 36
Longitude(°W)
76 74 72 70 68 66 64

Figure 15

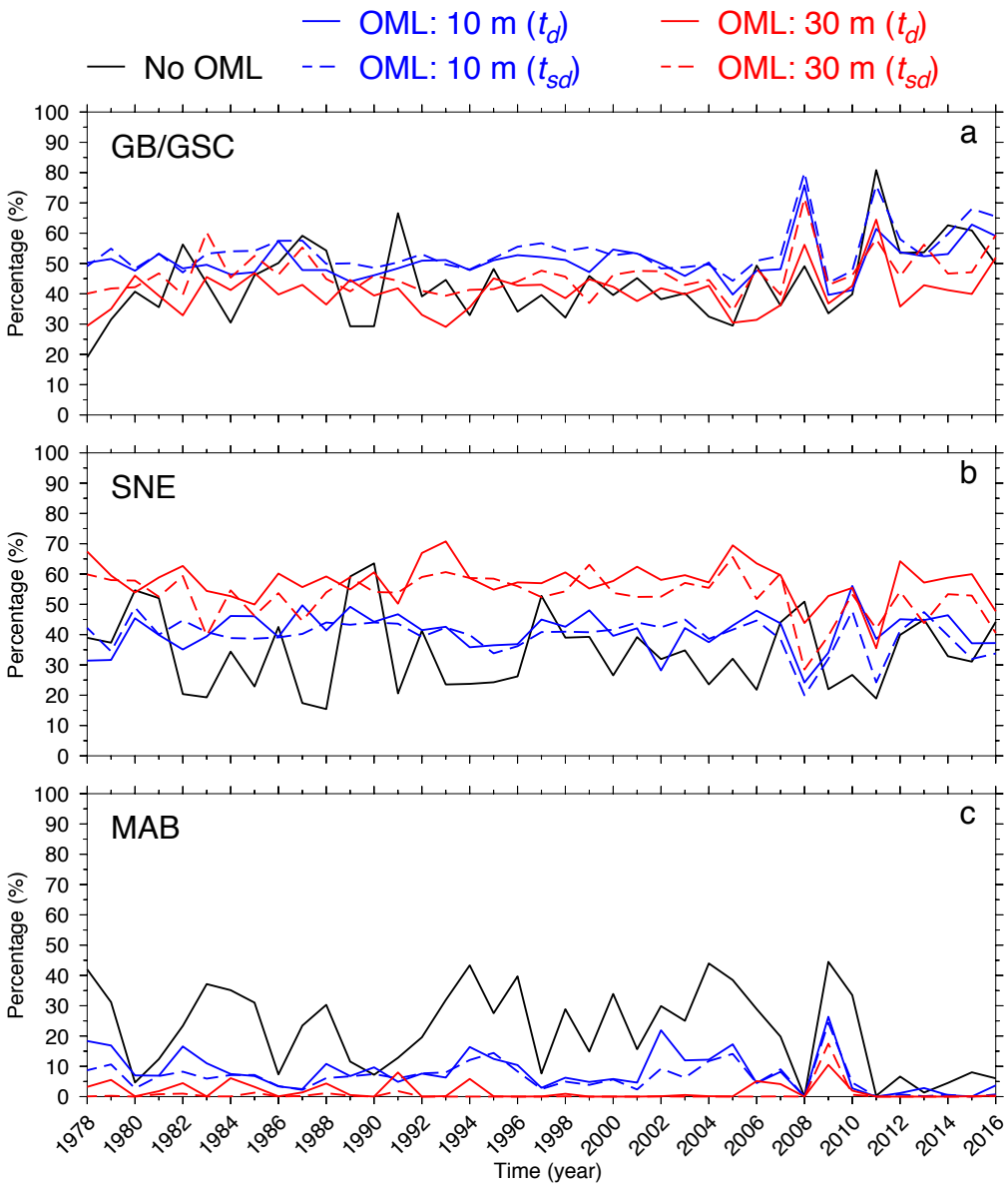
No OML
OML: 10 m (t_d)
OML: 10 m (t_{sd})
OML: 30 m (t_d)
OML: 30 m (t_{sd})
GB/GSC
a
SNE
b
MAB
c
Percentage (%)
Time (year)

Figure 16

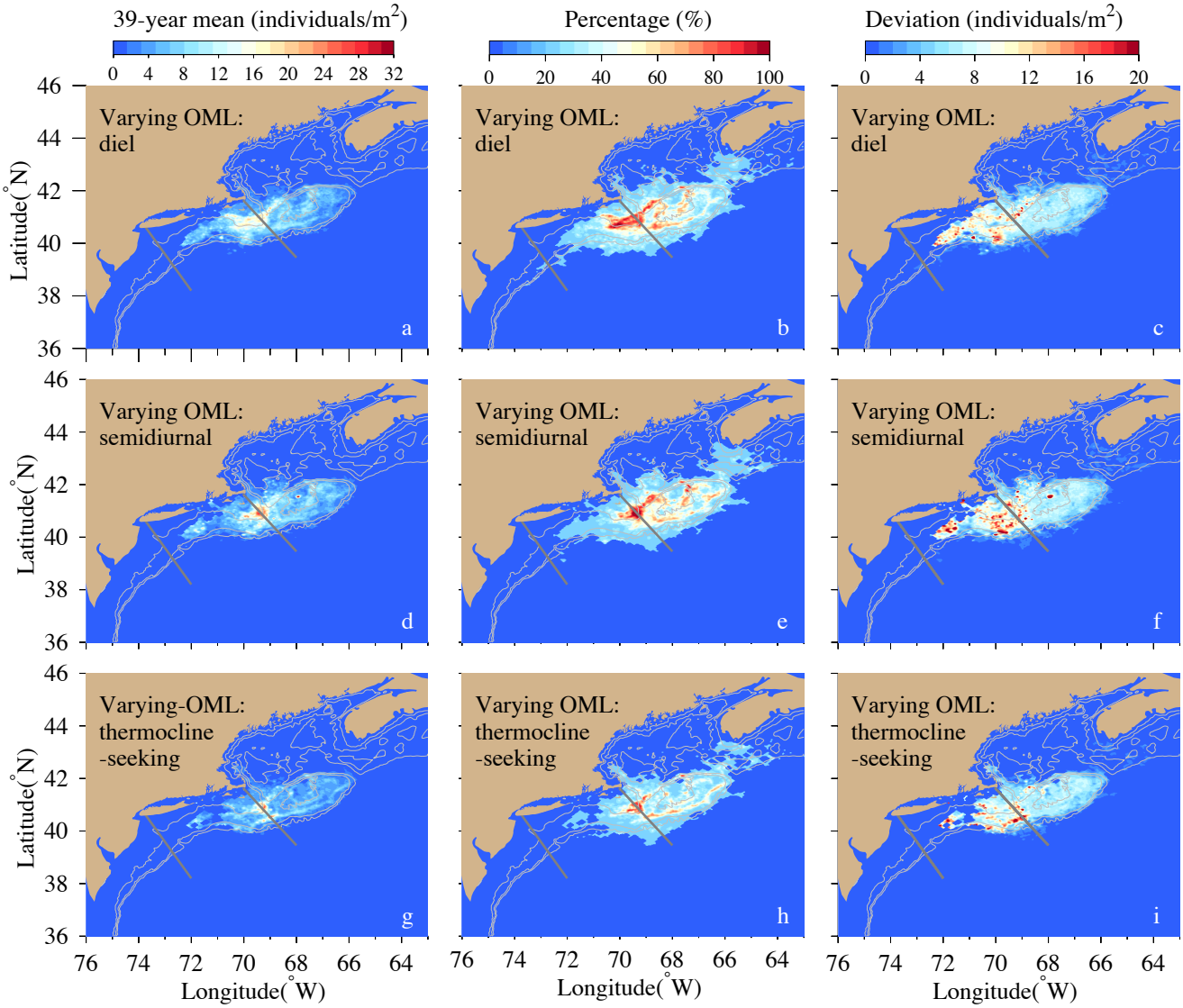
39-year mean (individuals/m2)
0 4 8 12 16 20 24 28 32
Percentage (%)
0 20 40 60 80 100
Deviation (individuals/m2)
0 4 8 12 16 20
Varying OML: diel
Varying OML: semidiurnal
Varying-OML: thermocline -seeking
Varying OML: thermocline -seeking
a
b
c
d
e
f
g
h
i
Latitude(°N)
Longitude(°W)
36 38 40 42 44 46
76 74 72 70 68 66 64

Figure 17

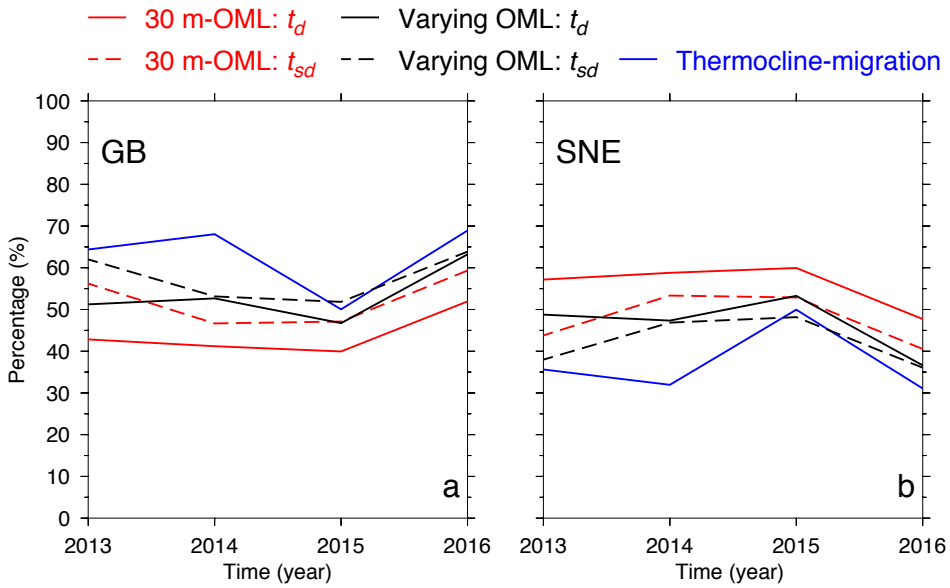
30 m-OML: t_d
Varying OML: t_d
30 m-OML: t_{sd}
Varying OML: t_{sd}
Thermocline-migration
GB
SNE
a
b
Percentage (%)
Time (year)
Time (year)
100
90
80
70
60
50
40
30
20
10
0
2013
2014
2015
2016

Figure 18

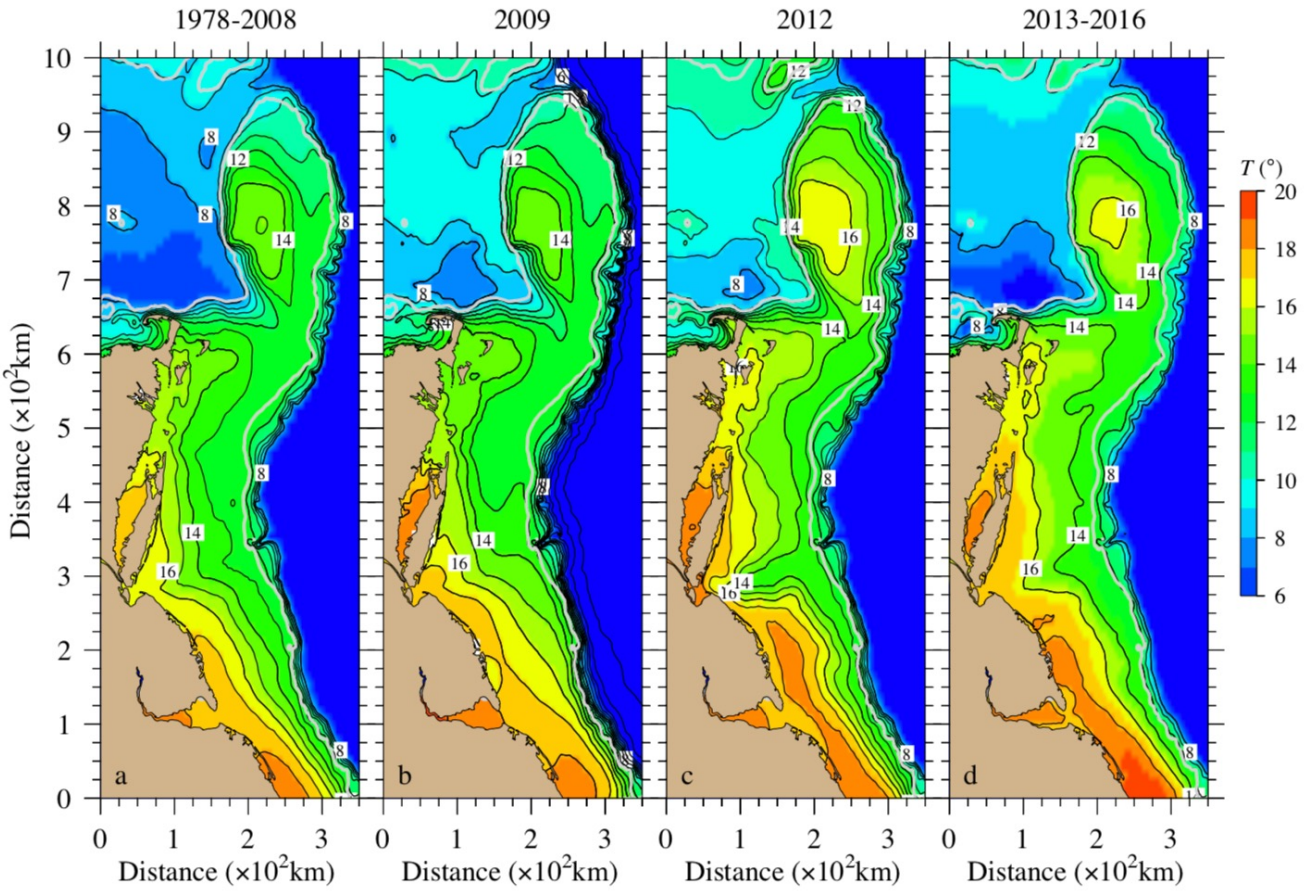
1978-2008
2009
2012
2013-2016
Distance (×10²km)
Distance (×10²km)
T (°)
a
b
c
d

Figure 19

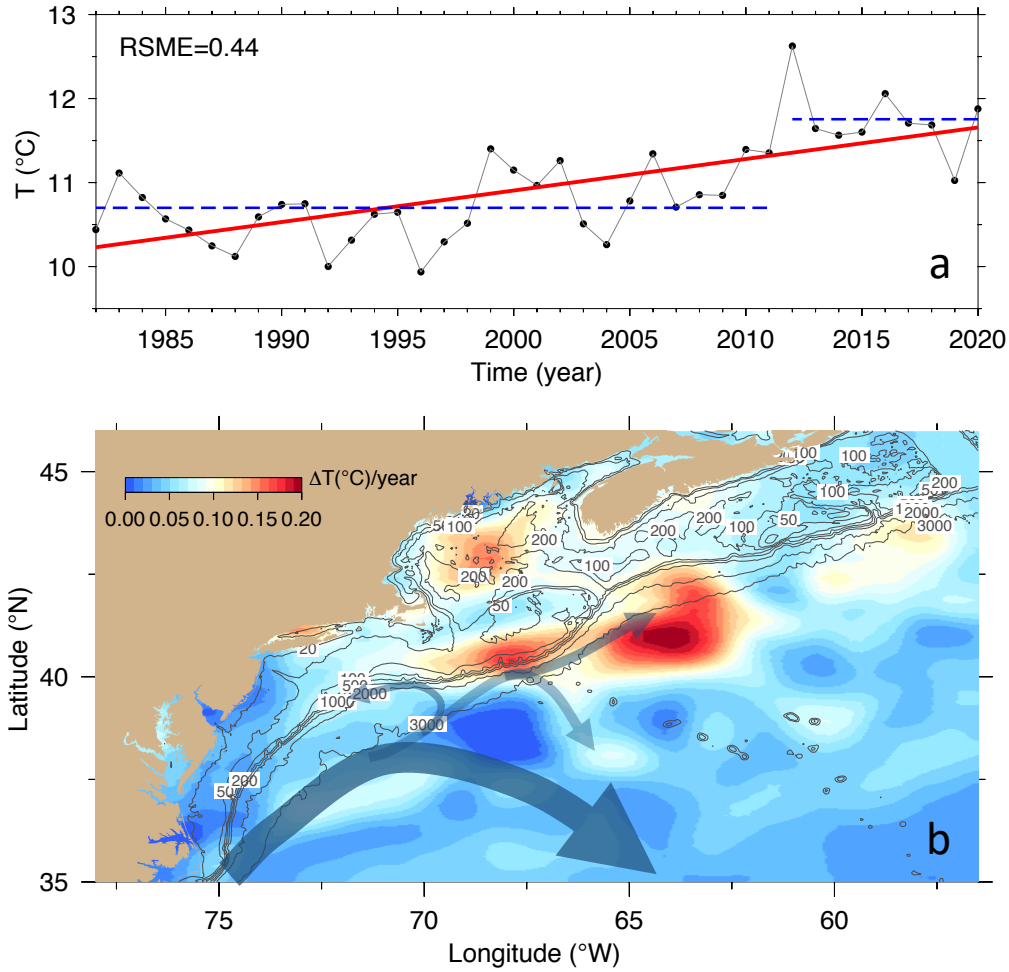
RSME=0.44
T (°C)
Time (year)
a
ΔT(°C)/year
0.00 0.05 0.10 0.15 0.20
Latitude (°N)
Longitude (°W)
b

Figure 20

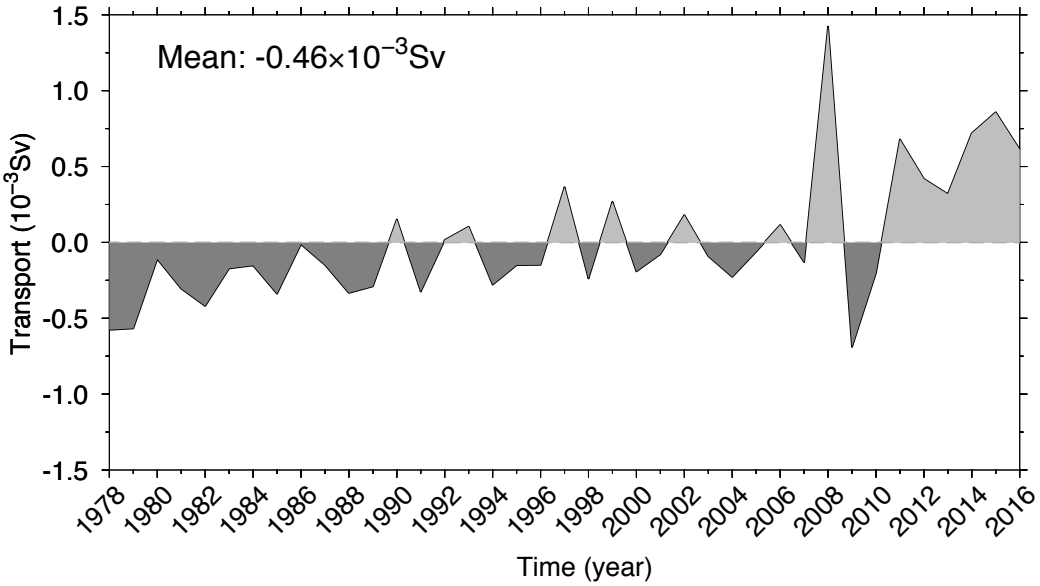
Mean: -0.46×10^{-3}Sv
Transport (10^{-3}Sv)
1.5
1.0
0.5
0.0
-0.5
-1.0
-1.5
1978
1980
1982
1984
1986
1988
1990
1992
1994
1996
1998
2000
2002
2004
2006
2008
2010
2012
2014
2016
Time (year)

Figure 21

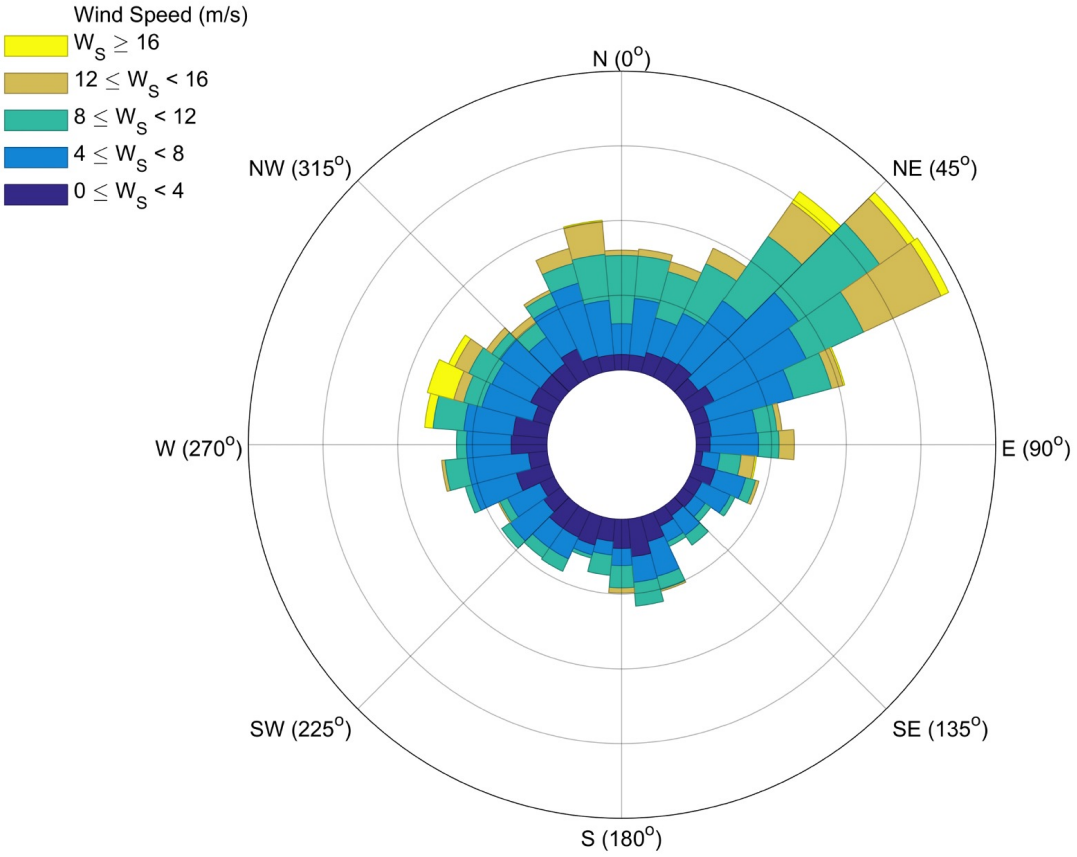
Wind Speed (m/s)
$W_S \geq 16$
$12 \leq W_S < 16$
$8 \leq W_S < 12$
$4 \leq W_S < 8$
$0 \leq W_S < 4$
N (0°)
NE (45°)
E (90°)
SE (135°)
S (180°)
SW (225°)
W (270°)
NW (315°)

Figure 22

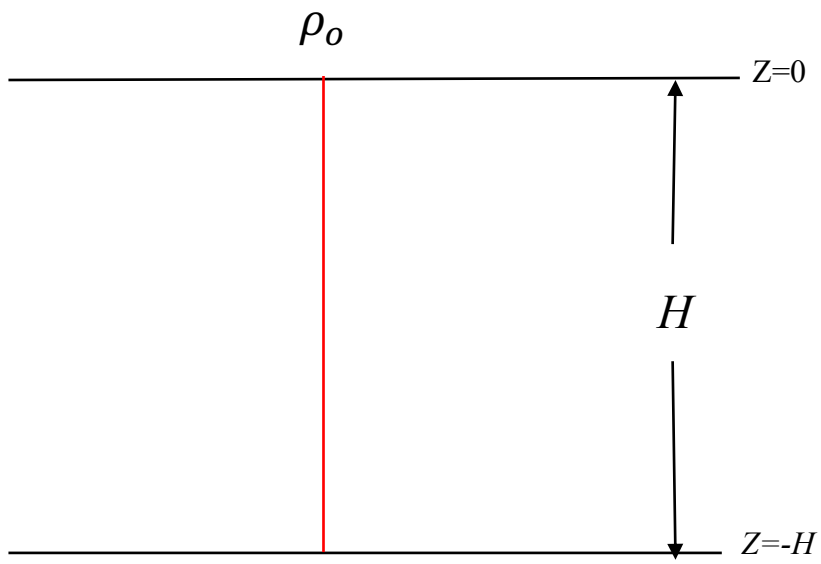

Figure A1

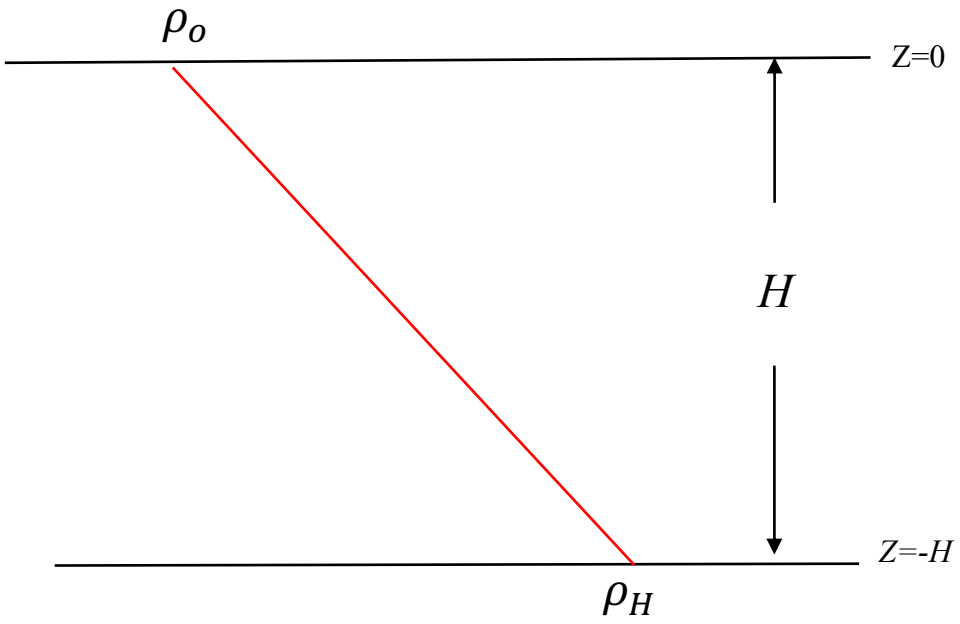

Figure A2

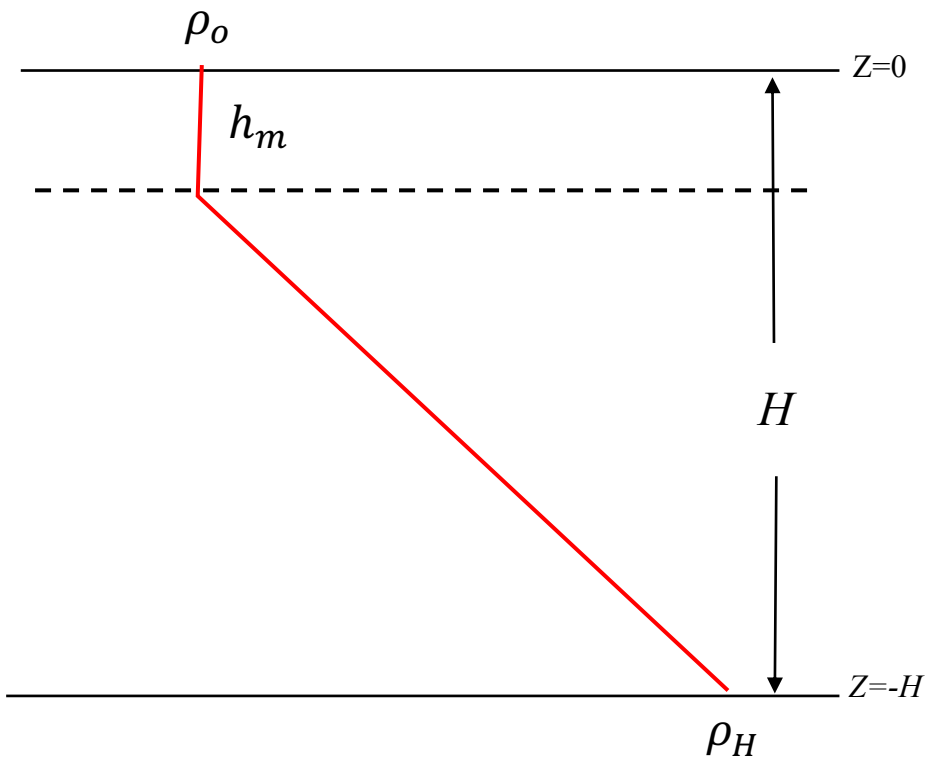

Figure A3

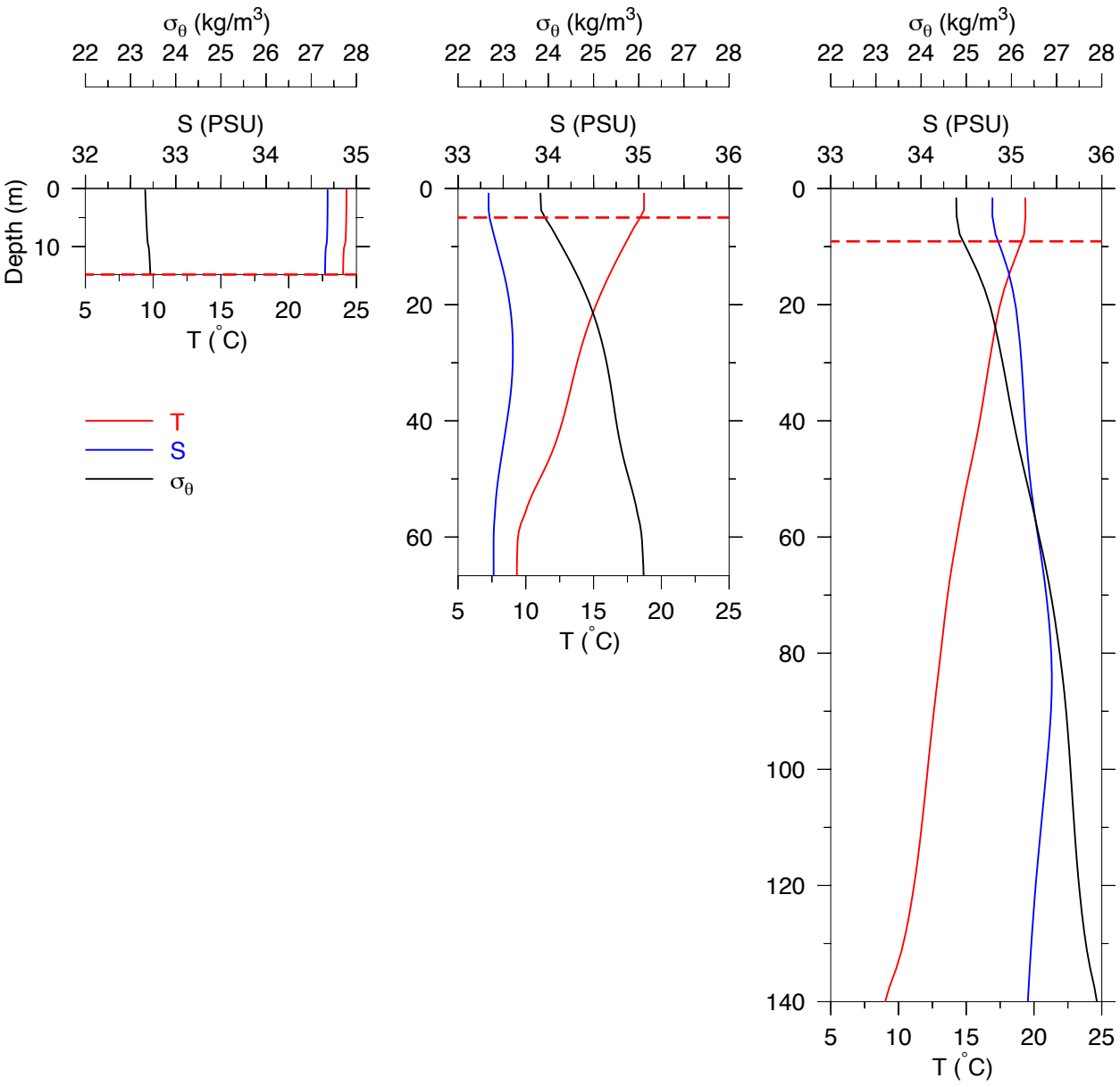
σθ (kg/m3)
22 23 24 25 26 27 28
S (PSU)
32 33 34 35
33 34 35 36
Depth (m)
0
10
20
40
60
80
100
120
140
5 10 15 20 25
T (˚C)
T
S
σθ

Figure A4